

NOAA Technical Memorandum ERL WPL-39



THE USE OF RADAR FOR STUDIES OF CLOUDS

E. E. Gossard

Wave Propagation Laboratory
Boulder, Colorado
July 1978

noaa

NATIONAL OCEANIC AND
ATMOSPHERIC ADMINISTRATION / Environmental
Research Laboratories



Digitized by the Internet Archive
in 2012 with funding from
LYRASIS Members and Sloan Foundation

<http://archive.org/details/useofradarforstu00goss>

NOAA Technical Memorandum ERL WPL-39

THE USE OF RADAR FOR STUDIES OF CLOUDS

E. E. Gossard

Wave Propagation Laboratory
Boulder, Colorado
July 1978



UNITED STATES
DEPARTMENT OF COMMERCE

Juanita M. Kreps, Secretary

NATIONAL OCEANIC AND
ATMOSPHERIC ADMINISTRATION

Richard A. Frank, Administrator

Environmental Research
Laboratories

Wilmot N. Hess, Director

NOTICE

The Environmental Research Laboratories do not approve, recommend, or endorse any proprietary product or proprietary material mentioned in this publication. No reference shall be made to the Environmental Research Laboratories or to this publication furnished by the Environmental Research Laboratories in any advertising or sales promotion which would indicate or imply that the Environmental Research Laboratories approve, recommend, or endorse any proprietary product or proprietary material mentioned herein, or which has as its purpose an intent to cause directly or indirectly the advertised product to be used or purchased because of this Environmental Research Laboratories publication.

TABLE OF CONTENTS

1.	INTRODUCTION	1
2.	EFFECTS OF THE ATMOSPHERE ON RADAR OBSERVATION	5
	Introduction	5
	Reflection and Refraction	6
	Absorption	6
	Scattering	7
	Scatter from clouds and precipitation	13
	Scatter from the clear-air	17
3.	VARIOUS RADARS AND THEIR POTENTIAL FOR CLOUD DETECTION	20
4.	RADAR REFLECTIVITY AND CLOUD CHARACTERISTICS	22
	Introduction	22
	Drop-size distribution - some special cases	22
	A general drop-size distribution function	24
	Methods for measuring drop-size in-situ	28
	Observation of drop-size distribution in natural clouds	29
	Observations of drop-size distribution in man-made clouds	31
	Observations of cloud reflectivity	33
	Conclusions	35
5.	RADAR ATTENUATION AND CLOUD OBSERVATION	36
	Introduction	36
	Attenuation of radar waves by small water drops	36
	Optical extinction by small water spheres	38
	A cloud parameter diagram	39

TABLE OF CONTENTS (cont'd)

Measuring Z and k	41
Analysis of errors	42
Conclusions	43
6. POLARIZATION AND SCATTERER CHARACTERIZATION	44
Introduction	44
Backscatter by non-spherical particles	46
Introduction	46
Theory	47
Geometry of scattering	51
Perfect sphere	54
Random orientation	55
Oblate spheroids	55
Prolate spheroids	57
Differential reflectivity of non-spherical particles	58
Attenuation by non-spherical particles	61
Scattering in an arbitrary direction	63
Conclusions and possible operational applications	64
APPENDIX	69
REFERENCES	113

THE USE OF RADAR FOR STUDIES OF CLOUDS

E. E. Gossard

NOAA/ERL/Wave Propagation Laboratory

Boulder, Colorado 80302

1. INTRODUCTION

This report addresses the ways in which cloud detecting radars might be of value at a weather observation station. From a survey of cloud physicists and modelers, the following suggestions seem to be relevant:

- a) If a cloud surveillance capability existed over a large area around a weather station, the local forecaster would have a picture of the distribution of solar insolation in the vicinity. This would clearly aid in temperature nowcasting and short-term forecasting. It should be of some aid in predicting where local storm development is most likely and as input to some forecasting models. It should provide a valuable supplement to satellite observations by providing details of local cloud types and their three-dimensional structure.
- b) In preparing flight plans for aircraft, and in landing operations, it would often be of value to know the spatial distribution of clouds and their density (especially when dealing with those aircraft restricted to VFR).

- c) When forecasting the dissipation of low stratus clouds or fog, the forecaster would benefit by knowing the existence and distribution of clouds above the fog layer. This is illustrated by Fig. 1-1b observed by Petrocchi and Paulsen (1966) using a vertically pointing TPQ-11 radar of 0.86 cm wavelength. There are two layers above the fog in this figure. There is a clear trend toward intensification of the important middle layer that would prevent dissipation of the fog and alter the usual forecast of burn-off time.
- d) Radars can also show the slope of advancing precipitation and thus they can provide a precise prediction of the onset of precipitation. This is seen in Fig. 1-2 which shows an approaching snowstorm descending at a rate of 5000 ft an hour. According to Petrocchi and Paulsen (1966), trends in intensity can also provide insight into the duration of a storm.
- e) Cloud radars can reveal evidence of strong wind shear as shown in Fig. 1-3. Such shear zones are of obvious interest around airports and may also imply strong turbulence.
- f) Given two frequencies, cloud radars may be able to monitor continuously the mass median drop-size and liquid water density in evolving cloud systems and thus aid in the prediction on the mesoscale of those that will become precipitating storms.

On the negative side, coverage by cloud radars seems to be rather unpredictable. The radar "cloud" often does not correspond to the visual cloud, and the radar echo cannot be related to the international cloud classification system.

According to Plank, et al. (1954), of 89 periods during which echoes were received slightly less than 50 percent of the echoes could be classed as echoes from internationally defined clouds. Furthermore, only about 47 percent of the visual clouds were detectable on a 1.25 cm wavelength radar. This is in good agreement with conclusions by Harper (1964) who made measurements with a 0.86 cm wavelength radar at Malvern. He reported that about 50 percent of high and low clouds and 75 percent of medium clouds in southern England give detectable signals. His observations indicate that radar is often unreliable as an indicator of true cloud bases and tops. The radar observations often reveal fall streaks, suggesting the presence of precipitation size particles and also suggest ice particles in clouds to be a factor in radar detection. Some dense water fogs are detectable by the fog tops are not defined by radar.

It seems reasonable to conclude that cloud detection radars can potentially play a useful role in weather observation. However, at the present stage they provide little quantitative information and the relation of radar echoes to visual clouds remains obscure. It is probably important to initiate some radar cloud research in order to clarify the relative importance of cloud radars. Past work in this field has emphasized the cloud

detection role of radars, and there is, probably little value in much further research of this kind. However, the effects of clouds on attenuation and depolarization have not been pursued as far as they might have been. Past emphasis has been mainly on research at vertical incidence where polarization experiments are very limited. However, even then some enhanced returns apparently due to orientation of ice crystals were noted.

New requirements posed by satellite systems increase the availability of radar components at very short wavelength and make it feasible to do multiple radar, multiple polarization, multiple frequency experiments. If combinations of reflectivity and attenuation observations can give quantitative measures of cloud liquid water content, drop density, and precipitation, or if polarization and/or cross-polarization can be used to delineate state throughout volumes of cloud and storm systems, the value of cloud radars at a weather station would be greatly enhanced. Furthermore, two or more separated radars equipped with Doppler can detect the radial component of the velocity of precipitation particles within storms and (with suitable processing) are capable of displaying the complete three dimensional particle motion field from which the three dimensional air motion can be estimated. K-band radars can, in principle, sense the particle fields at a much earlier stage in the storms evolution. Thus multiple frequency, multiple radar systems offer the hope of providing, not only information on the cloud microphysics, but of also providing the cloud dynamics to complement the microphysics.

In what follows the measurement by radars of a) reflectivity, b) attenuation and c) polarization will be examined in turn and specific recommendations for their uses will be made.

2. EFFECTS OF THE ATMOSPHERE ON RADAR OBSERVATIONS

Introduction

At microwave frequencies the refraction, absorption and scattering properties of the nonionized clear atmosphere result mainly from the fact that the water vapor molecule possesses an electric dipole moment. Of lesser importance, except for wavelengths near 5 mm, is the magnetic dipole moment of the oxygen molecule. Except near the absorption lines of water vapor and oxygen, the refractive index for microwaves can be considered to be essentially independent of frequency, and gaseous absorption can be considered to be negligible. For most purposes radar frequencies are deliberately chosen for which these conditions are satisfied. The real part of the refractive index n is then related to the ambient temperature, pressure, and humidity (e.g., see Bean and Dutton, 1968) as

$$(n-1) \times 10^6 = (77.6 P/T)(1 - 4810 e/T^2) . \quad (2-1)$$

In general the nonionized atmosphere can influence radar in several ways: by a) reflection b) refraction c) absorption by atmospheric gases d) absorption by hydrometeors e) scattering by dielectric inhomogeneities and f) scattering by hydrometeors.

Reflection and Refraction

Refraction and specular reflection have important effects on radar systems only when the propagating wave is incident on stratified atmospheric layers at very small angles of incidence. This case is important for surveillance systems in which the radar points nearly horizontally in the presence of atmospheric layers with large vertical gradients of temperature and/or humidity. However reflection and refraction effects seldom are important in radar studies of cloud structure or even the usual applications of radar to investigate the structure of the clear air.

Absorption

At microwave frequencies, gaseous absorption occurs in the neighborhood of water vapor and oxygen absorption lines in the spectrum. The absorption spectra for oxygen and water vapor in the microwave band is shown in Fig. 2-1 taken from Bean and Dutton (1968). Gaseous absorption is seldom important in atmospheric studies by radar because radar frequencies are usually chosen to minimize this kind of absorption.

On the other hand absorption by hydrometeors is important in many meteorological applications. However, for cloud studies it only becomes important at the very short wavelengths. For small spherical scatterers, whose size is much less than a wavelength, the Rayleigh approximation is applicable and the absorption crosssection Q_a of a single sphere is given by (e.g., see Batton, 1973)

$$Q_a = (\pi^2 D^3 / \lambda) [\operatorname{Im} \left(-\frac{m^2 - 1}{m^2 + 2} \right)] \quad (2-2)$$

where $m = n - ik$ is the complex index at refraction of the scatterer, e.g., water, λ is wavelength, and D is diameter of the sphere. The attenuation of the radar wave, due to hydrometeors, is the sum of their absorption and the loss of energy scattered out of the beam. The attenuation by clouds (as related to visibility) and precipitation (as related to rainfall rate) is shown in Fig. 2-2.

Scattering

For meteorological applications, scattering by both hydrometeors and by turbulence in the clear air is very important. A concise derivation of the radar equation, which includes the radar system parameters, is given in the Appendix. At this point it is necessary to introduce the concepts of "reflectivity" resulting from scattering, but they will be derived in terms of the incident electric field, and they will be presented independent of radar systems.

The electric moment per unit volume induced in a scatterer is

$$(4\pi)^{-1} E(\epsilon - \epsilon_0) \quad (2-3)$$

where ϵ is the (uniform) dielectric constant of the scatterer, ϵ_0 is the ambient dielectric constant of the propagation medium, E is the electric field in the scatterer. The total moment for a scatterer of volume V is then

$$f = (\epsilon - \epsilon_0)(EV/4\pi) . \quad (2-4)$$

The scattered field E_s at a distance r_s from a dipole of moment f is given by

$$E_s = \frac{k_s^2 f \sin\psi}{\epsilon_0 r_s} \exp(-i k_s \cdot \hat{r}_s) \quad (2-5)$$

where $k_s = 2\pi/\lambda_s$ is the wavenumber of the wave scattered in the direction \hat{r}_s , and ψ is the angle between the direction of polarization of the incident electric field and the direction of k_s .

For a homogeneous sphere of dielectric constant ϵ , the electric field E induced in the sphere is (e.g., Gans, 1912)

$$E = E_o \left(\frac{3}{2+\epsilon/\epsilon_0} \right) \exp i(\omega t - k_o \cdot \hat{r}_o) \quad (2-6)$$

where E_o is the magnitude of the incident electric field and ω is the radio-frequency in radians per second. The vectors \hat{r}_o and k_o are the range from the source and the wavenumber of the incident wave, and their dot product gives its phase at the scatterer. Therefore

$$E_s = \left\{ E_o \frac{k_s^2}{r_s} \left(\frac{D}{2} \right)^3 \frac{(\epsilon/\epsilon_0 - 1)}{\epsilon/\epsilon_0 + 2} \right\} \sin\chi \exp i(\omega t - k_s \cdot \hat{r}_s - k_o \cdot \hat{r}_o) . \quad (2-7)$$

where E_s is the scattered field at r_s and $V = (\pi/6)D^3$.

For atmospheric targets there are usually many scatterers within the radar pulse volume. It is convenient to assume a monodispersive drop size distribution whose drops are all of diameter D. This constraint will be relaxed later. Letting $N dr_{\sim o}$ be the number of drops in the position increment between r_o and $r_o + dr_{\sim o}$, Eq. (2-7) becomes

$$E_s = E_o \left(k_s^2 / 4\pi r_s \right) 3 KV \sin \psi \int_v N(r_o) \exp i(\omega t - k_s \cdot r_s - k_o \cdot r_o) dr_{\sim o} \quad (2-8)$$

where $K = (\epsilon/\epsilon_o - 1) / (\epsilon/\epsilon_o + 2) \approx (\epsilon - \epsilon_o) / (\epsilon + 2\epsilon_o)$ and $V = (4/3) \pi (D/2)^3$ is the volume of the spherical scatterer. But

$$k_o \cdot r_o + k_s \cdot r_s = k_s \cdot (r_s + r_o) + (k_o - k_s) \cdot r_o \equiv 2k_s \cdot r + \kappa \cdot r_o$$

where the definitions $\kappa \equiv k_o - k_s$ and $r \equiv (r_s + r_o)/2$ have been adopted. From Fig. 2-3

$$\kappa = 2k \sin(\theta/2) \quad (2-9)$$

where $k \equiv |k_s| = |k_o|$. Recalling that average power is proportional to $\overline{E E^*}$, where the overbar indicates time average, we have for the envelope of the scattered power

$$P_s = P_o k_s^4 9 |K|^2 V^2 \sin^2 \psi I / (4\pi r_s)^2 = P_o (k_s^4 / r_s^2) |K|^2 (D/2)^6 \sin^2 \psi I \quad (2-10)$$

where $I = \overline{\left| \int N(r_o) \exp(-i \kappa \cdot r_o) dr_{\sim o} \right|^2}$. Now suppose the number density distribution function $N(r_o)$ to be composed of a deterministic and a random

(in some sense) part, i.e., $N = \bar{N}(\tilde{r}_o) + \delta N(\tilde{r}_o)$. The deterministic part will in general lead to partial reflection from large scale gradients of N within the radar beam, and it will be ignored in the present context.

Then

$$I = \iint \overline{\delta N(\tilde{r}_1) \delta N(\tilde{r}_2)} \exp[i\kappa^*(\tilde{r}_1 - \tilde{r}_2)] d\tilde{r}_1 d\tilde{r}_2 \quad (2-11a)$$

$$I = \iint \overline{\delta N(\tilde{r}_o) \delta N(\tilde{r}_o + \tilde{l})} d\tilde{r}_o \exp(-i\kappa^* \tilde{l}) d\tilde{l} \quad (2-11b)$$

where \tilde{l} is the separation of a certain scatterer from some reference position \tilde{r}_o in the scattering volume. It is convenient to define a spatial correlation function

$$C(l) = \frac{1}{\delta N^2 V} \int_V \overline{\delta N(\tilde{r}_o) \delta N(\tilde{r}_o + \tilde{l})} d\tilde{r}_o. \quad (2-12)$$

To carry out the volume integration it is simplest to define a coordinate system relative to the transmission direction, i.e., from transmitter to the scattering volume V . Thus θ is the angle to the scattering element dV off the direction from transmitter to the center of the scattering volume, l is the separation of the scatterer from the volume center and ϕ is the azimuthal angle about the transmission direction. Therefore the differential volume element $d\tilde{v}$ is

$$d\tilde{v} = l^2 dl \sin\theta d\theta d\phi \quad (2-13)$$

so

$$I = \overline{\delta N^2} V \int_0^\infty \ell^2 C(\ell) d\ell \int_0^{2\pi} \int_{-\pi}^{\pi} [\exp(-ik\ell \cos\theta)] \sin\theta d\theta d\phi \quad (2-14a)$$

or

$$I = \overline{\delta N^2} V \frac{4\pi}{k} \int_0^\infty \ell C(\ell) \sin k\ell d\ell . \quad (2-14b)$$

The choice of ∞ as an upper limit for ℓ is justified by the assumption that $C(\ell)$ falls off fast enough so that the contribution for large ℓ is negligible.

A function often chosen for $C(\ell)$ because of its mathematical simplicity is

$$C(\ell) = \exp(-\ell/\ell_0) . \quad (2-15)$$

Then

$$I = \overline{\delta N^2} V \frac{\frac{8\pi\ell_0^3}{(1+\ell_0^2 k^2)^2}}{} , \quad (2-16)$$

a result first obtained by Booker and Gordon (1950).

It is easy to establish the relation of scattered power to the power spectrum $E(k)$ of the scatterers by recalling the relation of $E(k)$ to the correlation function, i.e., the line spectrum

$$\phi_1(k) = \frac{2}{\pi} \int_0^\infty C(\ell) \cos k\ell d\ell , \quad (2-17)$$

where ℓ is scalar separation of scatterers along a line. Choosing $C(\ell)$ exponential as before,

$$\phi_1(\kappa) = \frac{2}{\pi} \frac{\ell_o^3}{1 + \ell_o^2 \kappa^2} . \quad (2-18)$$

However, Kovasny et al. (1949) pointed out that the three dimensional spectrum is related to the one dimensional spectrum of isotropic, homogeneous fluctuations such that

$$\phi_3(\kappa) = -\kappa \frac{\partial \phi_1(\kappa)}{\partial \kappa} . \quad (2-19)$$

Therefore

$$\phi_3(\kappa) = \frac{\overline{\delta N^2}}{\pi} \frac{\kappa^2 \ell_o^3}{(1 + \ell_o^2 \kappa^2)^2} . \quad (2-20)$$

Furthermore, if the scatterer concentration fluctuations are isotropic, the spectrum of vector ζ is related to the spectrum of scalar κ simply as [see e.g., Bolgiano (1958)]

$$\phi(\zeta) = \frac{\phi_3(\kappa)}{4\pi\kappa^2} = \frac{\overline{\delta N^2}}{\pi^2} \frac{\ell_o^3}{(1 + \ell_o^2 \kappa^2)^2} \quad (2-21)$$

Comparing (2-16) and (2-20, 21) it is readily seen that

$$I = 8\pi^3 V \phi(\zeta) = 2\pi^2 V \frac{\phi_3(\kappa)}{\kappa^2} = -2\pi^2 V \frac{1}{\kappa} \frac{\partial \phi_1(\kappa)}{\partial \kappa} \quad (2-22)$$

This remarkably simple relationship between the scattered power and the spectrum of the scatterers is perfectly general as pointed out by Villars

and Weisskopf (1954). Thus, for Kolmogoroff turbulence in the inertial subrange, one can simply insert the $\kappa^{-5/3}$ dependence for ϕ_1 and ϕ_3 and arrive at a $\kappa^{-11/3}$ dependence for I .

Scatter from Clouds and Precipitation

In calculating the scatter from cloud and precipitation particles it is usually assumed that the scatterer concentration is random in the sense that they are Poisson distributed, i.e., the particle concentration in neighboring parcels is completely uncorrelated where the meaning of "parcel" is an atmospheric volume of size approximately $(\lambda/2)^3$. If the number of scatterers $\delta N(\tilde{r}_1) d\tilde{r}_1$ is independent of $\delta N(\tilde{r}_2) d\tilde{r}_2$, the mean of the product in (2-11a) is zero except when $r_1 = r_2$; then,

$$I = \int_v [\overline{\delta N(r) dr}]^2 = \int_v \bar{N}(r) dr = N_T , \quad (2-23)$$

the total number of drops in the volume. That the variance is equal to the mean follows from the assumption of a Poisson distribution.

Then from Eq. (2-10)

$$P_s = P_o \frac{k_s^4}{(4\pi)^2 r_s^2} |K|^2 (D/2)^6 \bar{N}_T \quad (2-24)$$

which is just the product of the power scattered by a single drop and the total number of drops. A scattering cross-section σ is often defined as

$$P_s = \frac{P_o \sigma}{4\pi r_s^2} \quad (2-25)$$

so

$$\sigma = 4\pi k_s^4 |K|^2 \left(\frac{D}{2}\right)^6 \bar{N}_T = (\pi^5 / \lambda^4) |K|^2 D^6 \bar{N}_T. \quad (2-26)$$

Of course, in the case of cloud or precipitation particles the number distribution is not adequately represented by a single diameter D as assumed above. Instead the population of drops in the volume is represented by some type of size distribution N_D , where the number of drops in the size interval D to $D+dD$ is $N_D dD$. The total number of drops in the volume is then

$$N_T = \int_0^\infty N_D dD. \quad (2-27)$$

The total reflectivity is therefore proportional to

$$Z_T = \int_0^\infty N_D D^6 dD. \quad (2-28)$$

In order to distinguish this quantity from the reflectivity η , it is called the "reflectivity factor" Z (or Z_T when it is desirable to distinguish total Z from its value for a limited range of drop sizes). Thus, defining the reflectivity as

$$\eta = \int_0^\infty N(D) \sigma(D) dD = \frac{\pi^5}{\lambda^4} |K|^2 \int_0^\infty N(D) D^6 dD \quad (2-29)$$

we find

$$\eta = (\pi^5 |K|^2 / \lambda^4) Z_T \quad (2-30)$$

which is the usual expression for reflectivity from clouds and precipitation found in all textbooks.

The possibility that number density in neighboring parcels is not completely uncorrelated in precipitation was considered briefly by Goldstein and by Seifert in Kerr (1951) and rejected as an important consideration. However, it is not so evident that a coherent (Bragg) scatter is negligible in clouds, where number densities can be as high as 1000 cm^{-3} , and this possibility was considered from a theoretical standpoint by Smith (1964), by Naito and Atlas (1964) and by Chernikov (1968). The subject was apparently never pursued further because of the difficulty of measuring cloud number density spatial spectra, which Eq. (2-22) shows to be the decisive factor in the relative importance of incoherent vs. Bragg scatter from clouds. Equation (2-24) shows that incoherent scattered power has an inverse 4th power wavelength dependence, so short wavelength radars favor the incoherent return. If the cloud water spatial spectrum is approximately that of a passive scalar mixed by mechanical turbulence, $\phi(\zeta)$ should vary as approximately $\lambda^{11/3}$, so the scattered power should fall off only slightly with increasing wavelength. Until recently most radars used for tropospheric weather observation had wavelengths of 30 cm or less and cloud returns might be expected to be dominated by incoherent backscatter. With the modern use of radars at several meters

wavelength for sounding the clear (and cloudy) atmosphere, the question should be reexamined.

In the case of a cloud at saturation the question arises as to whether condensation will lead to more drops or to growth of existing drops or both. The answer probably depends on the number and kind of condensation nuclei (CCN) present and the degree of super saturation. The question can be largely avoided by dealing with liquid water content rather than number density. Thus a distribution function M_D for mass of liquid water can be defined such that the total mass of liquid water

$$M_T = \int M_D D^3 dD \quad (2-31)$$

and the correlation function analogous to (2-12) is

$$C(\ell) = \frac{1}{\delta M^2 V} \int \overline{\delta M(\tilde{r}_o) \delta M(\tilde{r}_o + \ell)} d\tilde{r}_o \quad (2-32)$$

so Eq. (2-10) becomes

$$P_s = P_o k_s^4 9|K|^2 \rho^{-2} \sin^2 \psi I / (4\pi r_s)^2 \quad (2-33)$$

where

$$I = \overline{\delta M^2} V \frac{4\pi}{K} \int \ell C(\ell) \sin \kappa \ell d\ell . \quad (2-34)$$

Scatter from the Clear Air

If we consider scatter from the molecules of the clear air, it is evident that the parcel to parcel variations in the Poisson sense will all be averaged out because the scale of molecular interaction is so small (a few molecular diameters at most) while the volume of interest is $\sim(\lambda/2)^3$. The only remaining contribution to the variance is that resulting from processes capable of organizing the scatterer concentration on scales of $\lambda/2$ or larger such as atmospheric turbulence. If there is variation of dielectric on this scale the incident electric field will polarize small volumes dV which deviate from the average by $\delta\epsilon$ and each small element will behave like a dipole of moment $(E/4\pi)\delta\epsilon dV$. For small deviations in ϵ , $3K \approx (\delta\epsilon/\epsilon_0)$ is the equivalent of changes in scatterer number concentration $\delta N dV$, so Eq. (2-10) gives

$$P_s = P_o [k_s^4 / (4\pi r_s)^2] \sin^2 \chi I \quad (2-35)$$

where $I = \left| \int_V \frac{\delta\epsilon}{\epsilon_0} (r_o) \exp(-ik \cdot r_o) dr_o \right|^2$

As before

$$I = 8\pi^3 V \phi_{\epsilon}(\kappa)$$

where $E(\kappa)$ is now the spectrum of atmospheric dielectric fluctuations. It is often more convenient to express the problem in terms of the refractive index m given by

$$m = \sqrt{\mu\epsilon}$$

where the permeability μ is essentially unity for air. But $m = n - ik \approx n$ except near absorption lines in the spectrum, so $\epsilon \approx n^2$ and $\delta\epsilon \approx 2n\delta n$.

Therefore

$$\overline{\delta\epsilon(r) \delta\epsilon(r-\ell)} \approx 4 \overline{\delta n(r) \delta n(r-\ell)} \quad (2-37)$$

since $\epsilon_0 \approx n_0 \approx 1.0$. Thus, using Eq. (2-20), we see that

$$\phi_\epsilon(\kappa) = 4\phi_n(\kappa)$$

where $\phi_n(\kappa)$ is the spectrum of n . Therefore

$$P_s = P_o V \frac{8\pi^4}{\lambda^4} \frac{\sin^2 \chi}{r_s^2} \frac{\phi_n(\kappa)}{\kappa^2}. \quad (2-38)$$

Thus

$$\eta = \frac{32\pi^5}{\lambda^4} \sin^2 \chi \frac{\phi_n(\kappa)}{\kappa^2} \quad (2-39)$$

analogous to Eq. (2-30).

Another parameterization that has been found convenient uses the structure parameter of refractive index C_n^2 which is most easily defined in terms of the structure function $D_n(\ell)$ given by

$$D(\ell) \equiv [\delta n(r) - \delta n(r-\ell)]^2 . \quad (2-40)$$

In the inertial subrange of homogeneous, isotropic turbulence it is found that

$$D_n(\ell) = C_n^2 \ell^{2/3} \quad (2-41)$$

where C_n^2 is a proportionality constant called the structure parameter.

Ottersten (1969) shows that Tatarskii's (1961) exposition leads to the conclusion that the one dimensional spectrum

$$\phi_1(k) \approx (1/4) C_n^2 k^{-5/3}$$

in the inertial subrange of homogeneous, isotropic turbulence. It has further been demonstrated by Kovasznay et al. (1949) and Bolgiano (1958) that the one dimensional scalar spectrum and the 3-dimensional scalar spectrum are related by

$$\phi_3(k) = -k \frac{d\phi_1(k)}{dk} . \quad (2-42)$$

Thus $\phi_1(k) \approx (1/4) C_n^2 k^{-5/3} = (3/5) \phi_3(k)$, so

$$\eta = \pi \left(\frac{5}{6}\right) \left(\frac{2\pi}{\lambda}\right)^4 C_n^2 k^{-11/3} \sin^2 \psi . \quad (2-43)$$

Therefore, three primary measures of atmospheric scatter are widely used — Z , η and C_n^2 depending on the nature of the scattering problem to be solved; the scattering cross-section σ is perhaps more widely used for single discrete targets. Various existing radars will now be analyzed in terms of these quantities.

3. VARIOUS RADARS AND THEIR POTENTIAL FOR CLOUD DETECTION

It is of obvious interest to compare the Z values of various cloud types with the minimum detectable Z of various radars. The starting point of such a comparison is either Eq. (A24a) or (A24b) of the Appendix. Here Eq. (A24b) will be used. Obviously, the minimum detectable Z depends on the radar parameters P_t , A_e , $(P_r)_{\min}$ and λ . It also depends on the range, r , and range resolution Δ . For a pulse radar, P_t and $(P_r)_{\min}$ are usually expressed as peak powers although average powers are readily used if the pulse-repetition period T and the pulse length τ are known.

For single-pulse processing

$$(P_r)_{\min} = k_B T_e B \quad (3-1)$$

if the noise is uniformly distributed over the receiver bandwidth B . Here $k_B = 1.375 \times 10^{-23}$ is the Boltzman constant. The quality of the receiver can be either expressed in terms of the "effective noise temperature," T_e , or the receiver noise figure, F , related to the noise temperature by

$$F = \frac{T_e + 290^\circ}{290^\circ} \quad (3-2)$$

F is often given in dB.

Table I presents the resulting calculations of Z_{\min} and n at a range of 10 km for many radars including the 3.2 cm radar and the FM-CW radar of the Wave Propagation Laboratory. Single pulse processing is not

relevant to the FM-CW radar so a range cell size of 100 m and a sweep length of 50 milliseconds was chosen in calculating $(P_r)_{\min}$.

It is immediately evident that cumulonimbus, cumulus congestus and Hawaiian orographic clouds should be detected by almost all radars at a range of 10 km. However, fair weather cumulus and continental cumulus should be detected only by the Defford and Wallops Island 10-cm radars and by the 0.86 cm TPQ-11 and the CPS-9. Note that there is a fourth power dependence of Z_{\min} on λ , although η is independent of wavelength; therefore, the short wavelength radars have a very great advantage in the detection of targets consisting of small discrete spherical droplets.

Comparing Z values for the various clouds with the minimum detectable values shown in Table I, we see that most clouds would not normally be seen by the 3.2 cm wavelength radar listed in the Table at a range of 10 km based on single pulse processing alone. However, if longer pulse-lengths (e.g., 1-5 μ sec) were used and averages taken over many spectra, clouds such as those observed at South Park should be detectable. If the velocity spectra in clouds are narrow, the total processing gain to be realized from Doppler processing and averaging may amount to as much as 10 dB.

4. RADAR REFLECTIVITY AND CLOUD CHARACTERISTICS

Introduction

This section reviews past work on cloud detection by radar and summarizes some conclusions regarding the detectability of various clouds. Some special drop size distributions are analyzed, and one quite general form is discussed.

Drop-size distribution - some special cases

The results of measurements of cloud drop-size distributions prior to 1949 have been summarized by Best (1951). He concludes that the data fit the relation

$$1 - F = \exp [-(D/D_o)^n] \quad (4-1)$$

where F is the fraction of liquid water in drops of diameter less than D . He shows that the mean of values of n found by all investigators is 3.3. Furthermore, of the various kinds of mean, mode or median that might be chosen as D_o , Best finds that the median drop diameter (the size at which half the water is contained in larger drops) is most independent of n and of minimum measurable diameter in the sample.

If the cloud drop-size distribution obeys a Marshall-Palmer exponential, $N_D = N_o e^{-AD}$, where $N_D dD$ is the number of drops of diameter between D and $D + dD$. The total mass of water is then given by

$$M_T = \rho \frac{\pi}{6} N_1 \int_0^{\infty} D^3 e^{-\Lambda D} dD = \rho \frac{\pi}{6} N_o \frac{3!}{\Lambda^4}. \quad (4-2)$$

If D_o is mass median diameter, $\Lambda = 3.67/D_o$. Then the total number of drops per unit volume is given by $N_T = N_o D_o (3.67)^{-1}$ and the total liquid water content (LWC) is $M_T = \rho \pi N_o D_o^4 / (3.67)^4$. The water content in the drop-size interval dD is

$$M_D dD = dM = \rho \frac{\pi}{6} N_o D^3 e^{-3.67D/D_o} dD \quad (4-3a)$$

so the fractional water content in the interval dD is

$$dM/M_T = [(3.67)^4/6] (D/D_o)^3 e^{-3.67D/D_o} dD/D_o \text{ (for Marshall-Palmer).} \quad (4-4a)$$

This expression can be compared directly with dF , found from Eq. (1) to be

$$dF \equiv dM/M_T = 3.3 (D/D_o)^2.3 d^{-(D/D_o)^3.3} d(D/D_o) \text{ (for Best).} \quad (4-4b)$$

We are more interested in the fractional contribution to the total reflectivity factor Z by drops of different size. Note that $dM = \rho(\pi/6) D^3 N_D dD$ and, from the definition of Z ,

$$dZ = D^6 N_D dD. \quad (4-5a)$$

Therefore,

$$dZ = \rho^{-1} (6/\pi) D^3 dM . \quad (4-5b)$$

So from Eqs. (4-4a) and (4-4b) we find expressions for the fractional contribution to Z analogous to those for liquid water content M . They are plotted in Fig. 4-1. The contribution to reflectivity factor is evidently concentrated near the mass-median of the drop-size population. The total reflectivity factor Z_T is thus related to the mass median drop-size as follows:

$$Z_T = N_o \frac{6!}{(3.67)^7} D_o^7 = \frac{6! M_T}{\rho \pi} \frac{D_o^3}{\Lambda^3} \quad (\text{for Marshall-Palmer type exponential}) \quad (4-6a)$$

$$Z_T = \Gamma(\frac{3}{3.3} + 1) (6/\pi) (M_T/\rho) D_o^3 \quad (\text{for Best's distribution}) \quad (4-6b)$$

A general drop-size distribution function

The Marshall-Palmer and Best distributions are special cases (or nearly so) of a more general function usually called (see Deirmendjian, 1969) a "modified gamma distribution". It is given by

$$N_r dr = a r^\alpha \exp(-br^\gamma) dr = a' D^\alpha \exp(-b'D^\gamma) dD \quad (4-7a)$$

where, here, r is drop radius and $a' = a/2^{\alpha+1}$, $b' = b/2^\gamma$. This distribution is shown schematically in Fig. 4-2.

As seen above, the mass (or volume) median drop-size (D_o) is a convenient scaling length in radar scattering problems. In terms of D_o and G

$$N_D = a' D_o^\alpha (D/D_o)^\alpha \exp[-G(D/D_o)^\gamma] \quad (4-7b)$$

where G is readily identified as $b(D_o/2)^\gamma$. Integration of $N_D dD$ over all D gives

$$N_T = a' \gamma^{-1} D_o^{1+\alpha} G^{-(1+\alpha)/\gamma} \Gamma[(\alpha+1)/\gamma] \quad (4-8)$$

where N_T is the total number of drops per unit volume. The slope of the distribution is zero at $r = 0$, at $N = N_{\max}$ and at $r = \infty$. In Table II the drop size radius or diameter associated with the maximum of $N(r)$ is called r_c or D_c . At N_{\max} where $dN/dD = 0$

$$b = \frac{\alpha}{\gamma r_c^\gamma} \equiv \frac{G}{r_o^\gamma}$$

whence it is readily seen that

$$D_o = \left(\frac{\gamma G}{\alpha}\right)^{1/\gamma} D_c \quad (4-9)$$

Similarly,

$$M(D_1) = \rho \frac{\pi}{6} \int_0^{D_1} D^3 N_D dD \quad (4-10)$$

Using Eq. (4-7b) and integrating over all D

$$M_T = \frac{4}{3} \rho \pi a \gamma^{-1} G^{-(4+\alpha)/\gamma} \Gamma[(4+\alpha)/\gamma] 2^{-(4+\alpha)} D_o^{4+\alpha} \quad (4-11)$$

the mass of liquid water contained in drops for which $D < D_1$ is given by

$$M(D_1) = \frac{M_T}{\Gamma(\frac{4+\alpha}{\gamma})} \int_0^{x_1} x^{(4+\alpha-\gamma)/\gamma} e^{-x} dx \quad (4-12a)$$

$$= M_T [1 - e^{-x_1} \left(\frac{x_1^n}{n!} + \frac{x_1^{n-1}}{(n-1)!} \right) \dots x_1 + 1] \quad (4-12b)$$

in $n \equiv 4+\alpha-\gamma$ is integral and where $x = G(D/D_0)^\gamma$. Note also that $\Gamma(n+1) = n!$.

G is uniquely determined for given values of α and γ ; it is found from that value of x for which the mass $M(D) = 1/2$, so that half the volume (or mass of liquid water) lies in sizes less than D_0 . A plot of G is shown in Figure 4-3. From (4-7b) we see that the Marshall-Palmer distribution results when $\alpha = 0$, $\gamma = 1$. Then $G \equiv \Lambda = 3.67$ and $a' = N_0$. It is therefore no surprise that Eq. (4-8) then yields $N_T = a' D_0 (3.67)^{-1} \equiv \frac{a}{2} \Lambda^{-1}$ whence we identify N_0 with $a/2$. Then Eq. (4-11) becomes

$$M_T = \frac{4}{3} \rho \pi a G^{-4} \Gamma(4) 2^{-4} D_0^{-4} \quad (4-13)$$

in agreement with the above discussion of the Marshall-Palmer distribution.

The distribution of Best (Eq. 4-4b) does not reduce precisely to a special case of Eq. (4-7a). Note that $G \approx 0.5$ instead of unity when $\gamma = 3.3$ and $\alpha = 0.7$. Also, in his discussion of Eq. (4-7a), Deirmendjian chooses to constrain α to be integral.

Here, we are more interested in the reflectivity factor Z than in M so, as in Eq. (4-6a) of the previous section, we note that $dZ = D^6 N_D dD = (6/\rho \pi) D^3 dM$. Using Eq. (4-7b) and Eq. (4-9) and integrating over all D

$$dZ = (6/\rho\pi) M_T \Gamma^{-1}[(4+\alpha)/\gamma] G^{-3/\gamma} D_o^3 x^{(7+\alpha-\gamma)/\gamma} e^{-x} dx \quad (4-14a)$$

or

$$Z_T = \frac{6M_T D_o^3}{\rho\pi G^{3/\gamma}} \frac{\Gamma[(7+\alpha)/\gamma]}{\Gamma[(4+\alpha)/\gamma]} \quad (4-14b)$$

Some parameters that have been suggested for the modified gamma function are shown in Table II for selected aerosols and hydrometers. The values of r_c , N_T , α and γ are taken from Deirmendjian (1969) except as indicated, but the values of G , M_T , D_o , Z_T and σ have been calculated from those drop-size distributions from the relations (4-8), (4-9), (4-11). (The value of $r_c = 4 \mu m$ given by Deirmendjian for a Double-Corona cloud seems to be an error. In our Table II we have assumed that it should have been $r_c = 2 \mu m$.) For comparison with the Deirmendjian models, we have also calculated the corresponding quantities from the Marshall-Palmer distribution for rainfall assuming the coefficients found by Gunn and Marshall (1958) for various rainfall rates. They find

Rain	Snow
$\Lambda(m^{-1}) = 4.1 \times 10^3 R^{-0.21}$	$\Lambda(m^{-1}) = 2.29 \times 10^3 R^{-0.45}$
$N_o(m^{-4}) = 0.08 \times 10^8$	$N_o(m^{-4}) = 0.038 \times 10^8 R^{-0.87}$

in the Marshall-Palmer distribution, where $N_D = N_o e^{-\Lambda D}$. All lengths are in meters except rainfall rate R which is in $mm hr^{-1}$. In Table II, it has been assumed that $R = 1, 4$ and $16 mm hr^{-1}$ for light, moderate and heavy precipitation respectively.

In the following paragraphs, observed cloud drop-size parameters have been compiled and tabulated, and it will be seen that the Deirmendjian parameters drastically underestimate the total liquid water content measured in natural clouds. Better in-situ measurements combined with good radar measurements are obviously needed.

Methods for measuring drop-size in-situ

Most in-situ measurements of drop size distribution have been made in powered aircraft, because the instruments required are complicated and relatively heavy. Exceptions are the measurements made on Mt. Washington and those made from a sailplane and reported by workers at the National Center for Atmospheric Research (NCAR) near Boulder, CO. The advantage of the latter systems is that the air stream is relatively undisturbed.

The conceptually simplest method used is direct photography if an arrangement is achieved that allows an undisturbed sample of air to be photographed. Unfortunately this is difficult and the method is expensive requiring a great deal of time to collect and process enough data to represent a significantly large sample.

One of the oldest methods is to expose slides to the air stream and count individual drops and their sizes. Such slides may be coated with grease (Weickmann and aufm Kampe, 1953) or with soot (e.g., Breed et al., 1976). This method is fairly accurate, but it is slow and laborious, requiring the human measurement and counting of individual drops. The photography and slide collection methods are most accurate for drops larger than 100 μm .

An earlier method used extensively by Diem (1948) and by Boucher (1952) on Mt. Washington employed a cylindrical "impinger". It is probably the least reliable of the widely used techniques.

Two recently developed methods that are now becoming widely used, depend on the scattering properties of spheres for optical wavelengths. A simple natural example of such effects are the halos that some clouds produce around the solar disk. The instruments are called the Axially Scattering Spectrometer Probe (ASSP), best for particles 2-30 μm in diameter; and the Forward Scattering Spectrometer Probe (FSSP), best for particles 3-45 μm in diameter. Such instruments aboard sailplanes probably provide the best data that can be collected in quantity (Dye, 1973). Unfortunately the lack of power limits the mobility of the sailplane and makes it difficult to sample different parts of a cloud system rapidly.

Observations of drop-size distribution in natural clouds

In 1953 Weickmann and aufm Kampe reported measurements of drop-size spectra in cumulus clouds. Observations were made at many locations within the clouds and the drop-size spectra from all observations were compiled into average spectra for three cumulus types: fair weather cumulus (*cumulus humulis*), *cumulus congestus*, and *cumulonimbus*. Photographs of typical drop distributions are shown in Fig. 4-7. In addition to drop-size distributions that allow the median diameter D_0 to be calculated, the average liquid water content $M(\text{g m}^{-3})$ and the average number of drops are given.

The height distribution of cloud radii and of spectral spread are shown in Fig. 4-5. The drop size reaches a maximum at near cloud base. The total water content is concentrated in drops of much larger radius in cumulus congestus than in fair weather cumulus as shown dramatically in Fig. 4-6. This fact has important implications for cloud detecting radars. However, some caution in accepting these data as typical is suggested by the fact that the median diameters of the clouds investigated by Weickmann and aufm Kampe are much larger than those of other investigators, so the reflectivity factors may not be very typical.

Squires (1958) has compared clouds of maritime origin near Hawaii with cumulus clouds of continental origin in Australia. Multiple exposure samplers were used, and the drop-size concentrations showed spatial variations on scales down to 300 m or less. Clear patches were often found in even dense clouds. However, characteristic differences were found. Squires studied orographic clouds 600 m to 1500 m thick with updrafts of 0.1 to 0.25 m sec⁻¹, dark stratus clouds about 300 m thick, and cumulus clouds over the sea with updrafts at about 1 m s⁻¹. He compared the results of the maritime cumulus with Australian continental cumulus of similar size and found very significant differences. Maritime cumuli showed relatively low drop concentrations (45 cm^{-3}) when compared with the continental cumuli which contained about 228 drops cm^{-3} . The liquid water content was similar in both, so the drops in the marine clouds were significantly larger than their continental counterparts. The cloud characteristics as measured by Weickmann aufm Kampe and by Squires are compiled in Table III. Table IV summarizes aircraft observations over Germany reported by

Diem (1948). Figure 4-7 (from Boucher, 1952) shows cloud data collected at Mt. Washington along with Diem's aircraft observations.

In experiments at South Park, near Denver, Colorado, Knollenberg's Axially Scattering Spectrometer Probe (ASSP) was used to measure drop-size distributions. Soot-coated slide samples were also taken. The results were reported by Breed et al. (1976) in the Proceedings of the International Cloud Physics Conference. The authors reported drop number density, mean diameter \bar{D} of the drops and total liquid water content for five cases from both the ASSP and the slide observations. The results are shown in Table V. Assuming a Marshall-Palmer exponential distribution, D_0 has been calculated from \bar{D} , and Z has been calculated from Eq. (4-6a).

It is clear from the various observations tabulated here that the liquid water content of the Deirmendjian clouds is an underestimate of what has been measured in natural clouds. This is most clearly true of cumulus types, for which much observational data exist; there have been few in-situ observations in the corona producing clouds.

Observations of drop-size distribution in manmade clouds

In recent years there has been concern about the ways in which man's activity may affect the environment. One concern has centered on problems of heat and moisture "pollution" and the resultant modification of local climate. Thus cooling tower plumes associated with the various kinds of power generating plants have been studied and their modification of the environment examined. Huff (1972) and Agee (1971) have demonstrated that

snowfall is enhanced downwind of power plants. The physical explanation is not clear though mechanisms have been proposed (Hanna and Gifford, 1975). The drop size distribution within the plume is a critical factor in the physics. It is exceptionally difficult to measure in a plume because tower-mounted in-situ sensors are seldom feasible and aircraft-borne penetrations are expensive and too brief to provide really satisfactory data. It is therefore of interest to examine the utility of short wavelength radars (e.g., 8.6 mm) to probe plume structure remotely. The problem has also been studied by Ricks (1977).

Few data sets are available, and we use here data acquired by Pena (1977) from aircraft penetrations of a power plant plume at Keystone, Pennsylvania. The same data set was used by Ricks.

The drop size spectra are listed in Table VI along with the conditions under which the data were collected. We have used these data to calculate by numerical integration the total number of drops (N_T), the total volume of liquid particulates (VP) and the total reflectivity factor (Z_T). Because of the importance of the large drops ($Z \propto D^6$), the distributions have been extrapolated to infinite drop size by fitting an exponential distribution to the measured distribution at the large-drop tail of the spectrum. The results for Z values from manmade clouds are very similar to the values found in natural clouds, for example in South Park (see Table V), but they are almost 2 orders of magnitude larger than Z's found from the Deirmendjian distribution for cumulus, for example.

Observations of cloud reflectivity

Few radar observations of clouds are to be found in the literature; most observations reported have been confined to precipitating systems, primarily because of the radar wavelengths used. The status of cloud observations using millimeter wavelength radars prior to 1964 has been presented by Plank et al. (1954) and by Harper (1964). At that stage of technology radar was not an impressive tool for cloud observation.

Based on observations relating the percentage mass distribution by size to drop-size distributions as measured at Mt. Washington Observatory, Bartoff and Atlas (1951) undertook to relate median diameter to the radar reflectivity factor Z . They arrived at the following relationship between reflectivity factor, median diameter, and total water content M (where the subscript T is dropped from now on):

$$Z = 1.35 (6/\pi) D_0^{-3} (M/\rho) \times 10^{12} (\text{mm}^6 \text{ m}^{-3}) \quad (4-15)$$

where D_0 is in meters and M is g m^{-3} . Although Eq. (4-15) is empirical, it is similar in form to (4-6b). The difference between $\Gamma(3/n+1)$ and 1.35 is probably not significant. Of course, D_0 and M are not unrelated; in fact, Atlas (1954) finds

$$D_0(\text{m}) = 26.5 \times 10^{-6} M^{1/3}$$

so

$$Z = 0.048 M^2 (\text{mm}^6 \text{ m}^{-3}) \quad (4-16)$$

or $Z = 139 D_0^6 \times 10^{24} (\text{mm}^6 \text{ m}^{-3}) . \quad (4-17)$

If radar reflectivity is used to estimate D_o and M, Atlas estimates that Eq. (4-15) gives a standard error of estimate of only 6.5% for D_o and 21% for M. Equation (4-16) yields a standard error of 33% for M and Eq. (8) a standard error of 16% for D_o . Apparently these relations might be useful for some practical problems such as estimating visibility within clouds, but they are not accurate enough to test the microphysics of cloud models.

For advection fogs, Donaldson (1955) finds the following relationships corresponding to the cloud Eqs. (4-15, 16, 17):

$$Z = 3.26 D_o^3 M \times 10^{12} \quad \left\{ \begin{array}{l} + 34\% \\ - 53\% \end{array} \right. , \quad (4-18)$$

$$Z = 8.2 M^2 \quad \left\{ \begin{array}{l} + 115\% \\ - 53\% \end{array} \right. \quad (4-19)$$

and

$$Z = 2.7 D_o^6 \times 10^{24} \quad \left\{ \begin{array}{l} + 91\% \\ - 48\% \end{array} \right. . \quad (4-20)$$

In Table I, the Atlas-Bartoff relationship, (Eq. (4-15)), has been used to compute Z for the Weickmann aufm Kampe data and the Squires data. These may be compared with $\Sigma N_i \Delta D_i^6$ calculated from Squires' data.* For comparison, $N_T D_o$ has also been computed, and it is clear that the Atlas-Bartoff equation is better, though not dramatically better, and it might sometimes be useful to substitute information about N for information about M when computing Z.

* Squires' data are presented as drop size histograms in size increments of typically $\Delta D = 10 \mu\text{m}$.

Conclusions

Experience gained in the 1950's and 1960's does not demonstrate that radar reflectivity is a very useful quantity in the observation and study of clouds. However, with the advances in radar technology in the 1970's, and with the inclusion of dual-frequency attenuation measurements, dual polarization and Doppler, the utility of radars for cloud investigations should be re-evaluated.

There is a wide range in measured values of cloud drop size distributions. This is partly due to the variety of measurement methods used, but present evidence suggests that the large variation may be real. There has probably been some bias because most experimental programs have been aimed at storm and precipitation research, and aircraft penetrations have tended to occur under conditions prior to or during precipitation conditions. This may partly explain why larger drop sizes and higher Z values are found from in-situ measurements than are deduced from the Deirmendjian model.

Introduction

The previous section addressed the question of useful experiments we might do if we had a cloud detecting radar and considered what information might be available from reflectivity measurements alone. In this section we consider what information might be extracted if we had both reflectivity and attenuation measurements available from radars with different wavelengths. Such methods have been used with some limited success in studies of precipitation (Goldhirsh and Katz, 1974), but the problem is different (and in some ways simpler) if it were to be used with clouds. It could, in principle, provide a spatial picture of the drop-size distribution in a developing storm.

Attenuation of radar waves by small water drops

Attenuation of radar waves may result from gaseous absorption, particle absorption (say by water droplets) or from particles scattering energy out of the beam. If radar wavelengths are chosen which avoid the water vapor and oxygen spectral lines (say 3.2 cm and 0.86 cm) gaseous absorption can be considered small. If the water drops are very small compared with radar wavelength, the Rayleigh approximation for the scattering and absorption cross-sections gives (Battan, 1973 pg. 67):

$$Q_s = \frac{2}{3} \frac{\pi^5}{\lambda^4} |\kappa|^2 D^6 \quad (5-1a)$$

$$Q_a = \frac{\pi^2}{\lambda} I(-K) D^3 \quad (5-1b)$$

where D is drop-size diameter, $K = (m^2 - 1)/(m^2 + 2)$, m is the complex index of refraction, λ is radar wavelength and $I(-K)$ is the imaginary part of minus K shown plotted in Fig. 5-1. Obviously, for very small D as in clouds, the absorption cross-section is the important consideration.

Then k (the absorption coefficient) is the sum of the absorption cross-sections of all the particles within a unit volume; so

$$k = \sum_{\text{vol}} Q_a = \frac{\pi^2}{\lambda} I(-K) \int_0^\infty N_D D^3 dD \quad (5-2a)$$

where $N_D dD$ is the number of drops in the size interval from D to $D + dD$.

However, note that total mass of liquid water

$$M = \rho \frac{\pi}{6} \int_0^\infty N_D D^3 dD$$

so

$$k = \frac{6\pi}{\rho\lambda} I(-K) M \quad (5-2b)$$

independent of the drop-size distribution. Thus, for water clouds, attenuation provides a simple, direct measure of liquid water content, if temperature can be estimated so that $I(-K)$ is known. From Section 4 the reflectivity factor Z is given by:

$$Z = N_o \frac{6!}{(3.67)^7} D_o^7 \quad (\text{for Marshall-Palmer exponential}) \quad (5-3a)$$

$$Z = \frac{6}{\rho\pi} \Gamma(1.91) D_o^3 M_T \quad (\text{for Best's cloud drop-size distribution}) \quad (5-3b)$$

+3.67 D/D_o

where N_o = N_D e^{-3.67 D/D_o} and D_o is the mass median diameter (i.e., the drop-size above which half the liquid water is found). From (5-2b) and (5-3a,b) it is easy to verify that

$$D_o^3 = \frac{\pi^2}{\lambda} \frac{I(-K)}{\Gamma(1.91)} \frac{Z}{k} \text{ (Best)}, \quad D_o^3 = \frac{\pi^2}{\lambda} I(-K) \frac{(3.67)^3}{120} \frac{Z}{k} \text{ (Marshall-Palmer)}. \quad (5-4a,b)$$

If we consider the more general drop size distribution, Eq. (4-7a), we see from Eq. (4-14b) that

$$D_o^3 = \rho \pi / (6 M_T) G^{3/\gamma} \Gamma[(4+\alpha)/\gamma] / \Gamma[(7+\alpha)/\gamma] Z. \quad (5-4c)$$

Optical extinction by small water spheres

The extinction coefficient σ_{ext} is defined by the relation I/I_o = exp(-σ_{ext}r) where I is the intensity of the transmitted light at range r and I_o is the intensity at r = 0. If Q_e is the extinction efficiency of a drop, then the extinction from a single drop is Q_eA, where A = πa_o² and a_o is the radius of the crosssection of the spherical drop. For a distribution of drops of uniform size the extinction coefficient is σ_{ext} = N Q_e πa_o² ≡ N Q_e(π/4)D² where N is the number of drops per unit volume. For number density distribution N_D

$$\sigma_{ext} = (\pi/4) \int_0^\infty Q_e D^2 N_D dD \quad (5-5a)$$

(see Van de Hulst, 1957, pg 129). In the Mie scattering limit of drops very large compared with wavelength, which is the usual condition for optical

wavelengths in the visible portion of the spectrum, $Q_e \rightarrow 2$ if the absorption is relatively small; then

$$\sigma_{ext} = (\pi/2) \int_0^{\infty} D^2 N_D dD. \quad (5-5b)$$

It follows that

$$\sigma_{ext} = \frac{3 \Gamma(0.7)}{\rho} \frac{M_T}{D_o} \quad (\text{Best}), \quad \sigma_{ext} = 367 \frac{M_T}{\rho D_o} \quad (\text{Marshall-Palmer}) . \quad (5-6a,b)$$

Again, the result may be calculated for the modified gamma function using Eqs. (4-7b) and (5-5b) and we find

$$\sigma_{ext} = 3 \rho^{-1} M_T G^{1/\gamma} D_o^{-1} \Gamma[(3+\alpha)/\gamma]/\Gamma[(4+\alpha)/\gamma]. \quad (5-6c)$$

Cloud parameter diagram (CLOUDPAD)

The assumption that $Q_e = 2$ has been examined by Hodkinson (1966) and Jiusto (1974). They find that it actually varies from 1 to 2 depending on the detection angle and range to the scatterer.

From Eqs. (4-13), (4-14b), (5-2b) and (5-6c) it is clear that Z , k , D_o , M and σ_{ext} are inter-related in a simple way if γ and α are known (as, for example is the drop size distribution is exponential). Atlas and Ulbrich (1974) have made use of this fact and have constructed a "rain parameter diagram" (RAINPAD) describing the relationships between the above quantities and rain-rate R (mm hr^{-1}) assuming a Marshall-Palmer distribution

in which $\Lambda = 41 R^{-0.21}$ (cm^{-1}). For particles of precipitation size, the Rayleigh approximation is not necessarily valid. Atlas and Ulbrich therefore write $M = \ell A^\beta$ where $A = 10 k \log e = 4.34 k$ is attenuation in dB per unit distance; actually, they express A in dB km^{-1} . In the Rayleigh approximation $\beta = 1$. On the other hand, when the drops are very large with respect to wavelength $\beta = 3/2$ for a monodisperse size distribution. In general the functional behavior of β is quite complicated because the full Mie scatter calculation is needed and the drop size distribution must be known. Assuming a Marshall-Palmer distribution, Atlas and Ulbrich made the necessary calculations for $\lambda = 3.22 \text{ cm}$ and $T = 10^\circ\text{C}$. Their results are shown in Fig. 5-2. The inter-relationships are much simpler for clouds because the Rayleigh approximation is valid. We have calculated the corresponding "CLOUDPAD" shown in Fig. 5-3. On the cloud diagram R of course is not relevant. In the cloud case, the diagram can be very general if a dimensionless attenuation $A\lambda/I(-K)$ is defined and used as a parameter. The diagram then applies to all temperatures in the Rayleigh size range. In Fig. 5-3 an exponential drop size distribution was assumed but no assumption of a value for N_o is necessary.

If Z and k can be observed by radar, some of the most important cloud quantities such as liquid water content, drop size (D_o) and extinction coefficient can be monitored continuously in time and space about the radar. If extinction coefficient can be obtained optically, the observational errors can be estimated and the relevance of the assumed spectral functions could then be judged.

Measuring Z and k

Suppose we use two radars of different wavelengths, one having a wavelength that is essentially unattenuated and the other heavily attenuated. Then for the unattenuated radar the received power P_{r1} is

$$P_{r1} = \frac{C_1}{r^2} Z$$

and from the other

$$P_{r2} = \frac{C_2}{r^2} Z e^{-2 \int_0^r k dr}$$

where r is range and C_1 and C_2 are known constants depending on the radar parameters. Then it is easy to see that

$$Z = \frac{P_{r1}}{C_1} r^2 \quad (5-7a)$$

and

$$k = \frac{1}{2} d \ln(P_{r1}/P_{r2})/dr \quad (5-7b)$$

From Z and k the cloud information is readily calculated from (5-4a,b) and (5-2b).

Unfortunately Eq. (5-7b) depends on absolute calibrations of both radars to get C_1 and C_2 , so the ratio P_{r1}/P_{r2} cannot be as accurate as comparative measurements made by a single radar. However, a single radar can yield k if the gradients in Z are not large. To see this, write the

integral over k from some range r_o to $r_o + \Delta$ where Δ is some small increment of range over which backscattered powers are to be compared. Then

$$\int_{r_o}^{r_o + \Delta} k \, dr = -\frac{1}{2} \ln \frac{P_{r_o} r_o^2}{P_{r_o + \Delta} (r_o + \Delta)^2}. \quad (5-8a)$$

If k and Z can be considered constant over the increment Δ , this gives

$$k = \frac{1}{2\Delta} \ln \frac{P_{r_o} r_o^2}{P_{r_o + \Delta} (r_o + \Delta)^2}. \quad (5-8b)$$

Now the ratio of powers applies to a single radar so only relative power at different positions is needed, and relative powers can be measured quite accurately. However, (5-8b) requires that Z be constant over the increment Δ . Since Δ is approximately 1 km, this assumption would be violated often in severe storms, but in a cloud system this assumption may be better.

Analysis of errors

If we presume that careful calibration of the radars will allow absolute power to be observed to an accuracy of ± 3 dB then Eq. (5-7a,b) and Eq. (5-4a,b) lead to error bars on M shown in Fig. 5-4a. If relative powers for a single radar have an accuracy of ± 0.3 dB Eq. (5-8a) gives the much smaller error range shown in Fig. 5-4b.

However, it is to be remembered that the validity of (5-8b) depends on Z remaining constant over the range of Δ . In severe storms there are

many times when this approximation is not valid even when Δ is chosen as small as 1 km. However, in the case of cloud systems that are more-or-less stratiform, or of storms in the early stages of development, the approximation that Z is roughly constant over increments of a kilometer may be much more realistic. It is likely that both (5-7b) and (5-8b) will be useful, with (5-7b) used mainly through regions of large gradients of Z .

Figures (5-5a) and (5-5b) show the corresponding errors in D_o to be expected for average reflectivities of -20 and -30 dBZ if Z can be estimated to an accuracy of ± 3 dBZ and $P_{r_o}/P_{r_o+\Delta}$ is known to ± 0.3 dB. We see that regardless of average reflectivity, the expected range of error is about $\pm 25\%$ which is probably not bad for many purposes since the range of D_o is so great.

Conclusions

In some ways clouds are nicer to work with than precipitation because the Rayleigh approximation can be used.

We see from Eq. (5-2a) that there is almost a factor of four difference in the attenuation of 3.2 cm radars and 0.86 cm radars. This should be enough difference to provide valuable information on spatial drop-size distribution and on its evolution. If a 10 cm radar were used, its waves could be considered as unattenuated and even better quantitative observations could be made. This kind of information could be of great value in understanding the microphysics of nucleation and precipitation. As an aid to

short-term forecasting at a Weather Service site, a forecaster might find it of value to watch for a rapid growth in D_o^3 (by watching Z/k) as a predictor of place and time of the onset of local precipitation.

6. POLARIZATION AND SCATTERER CHARACTERIZATION

Introduction

One of the impressive results of past radar cloud observations was the conclusion that high reflectivities in clouds were often associated with the presence of ice particles. More recently measurements of signals from satellites received on two polarizations often show significant signal in the cross-polarized channel even when there is little attenuation along the path. These observations could result from the polarizing effects of ice particles located somewhere on the path. Finally, cloud studies with radars have always produced cases for which there was significant backscatter from the apparently clear air. Some of these observations undoubtedly resulted from backscatter from turbulent inhomogeneities in the dielectric structure of clear air, but some of them might well result from enhanced backscatter from particles having a favorable alignment relative to the radar's polarization. The depolarization of satellite signals under conditions that occasionally are visually "clear" suggests that such events may be associated with ice crystals.

Additional support for this hypothesis comes from observations made with the WPL FM-CW radar pointing vertically. Strong and consistent

returns were observed at Fraser, Colorado from particles identified as ice blown off the peaks and ridges surrounding the site. An example is shown in Figure 6-1, in which both cloud particles and dielectric backscatter are shown. The dielectric backscatter is seen in the breaking wave structure faintly visible at a height of 2 km. The identification of the scattering particles was substantiated by simultaneous lidar observations.

Immediately we are presented with a mystery, of sorts, if we assume an expression similar to (Eq. A17) to be valid, because $K \equiv (m^2 - 1)/(m^2 + 2) \approx 0.93$ for water and only 0.20 for ice. The situation is even more drastic for snow because $K/\rho \approx$ constant and the density of snowflakes is only about 0.05 that of ice. Thus $K_{\text{snow}} = 0.05 K_{\text{ice}}$, and we would expect water drops to be much more effective scatterers than ice or snow. A possible explanation lies in polarization effects and the possibility that ice particles are often water coated. Growth and nucleation processes may also be important because particles with ice centers may grow to drop-sizes relatively large compared with coexisting water drops.

These observations suggest that it is imperative that more information be acquired on the inter-relationship between cloud types and radar backscatter; they demonstrate the potential importance of radar as an observational tool in a weather observing facility but emphasize the gaps in present knowledge that prevent its use in a quantitative and explicit way.

The observational results summarized above suggest an experimental program in which radar polarization might be exploited to fill in some

of the crucial information gaps.

Backscatter by non-spherical particles

Introduction

There has been an upsurge of interest in methods of calculating the polarization effects of non-spherical scatterers because of the anomalous depolarization events that are now recognized to occur commonly on earth-satellite paths. There are three primary ways in which the effect of scatterer shape on incident radiation may be analyzed. The theory of Gans (1912) is an amplification and extension of Lord Rayleigh's earlier theory (1881) for scattering from small spheroids. With the availability of computers, scattering theories based on Waterman's (1965) "extended integral equation" technique have been used (e.g., Bringi and Seliga, 1977) to treat non-spherical scatterers with diameters up to about 3λ . It provides an exact solution, but computers are generally needed for solution of the transition, or T-matrix. Finally, numerical solution for the scattering from bodies of arbitrary composition and shape is possible by dividing the scattering volume into incremental volume elements and matching the (complex) boundary conditions at all inter-volume-element boundaries. Only the Gans method provides results parametrically simple enough to make conceptually general statements about the effects of non-sphericity on scattering.

Theory

It is presumed in Gans theory that a uniform plane electromagnetic wave intercepting an ellipsoid excites dipole moments that can be resolved into three components along the orthogonal axes of the ellipsoid. The length of the axes are presumed small compared with the wavelength, and higher multi-pole moments are neglected. The Gans theory has been adopted by Atlas, Kerker, and Hitchfeld (1953) to deduce some effects of scatterer shape on radar backscatter.

The electric moment per unit volume induced in the scatterer is $E (m^2 - m_0^2)$ so the total moment is (see Section 2)

$$f = m_0^2 EV (m^2/m_0^2 - 1)/4\pi \quad (6-1)$$

where V is volume of the scatterer, m is its refractive index, m_0 is the refractive index of the propagation median, and E is the electric field induced in the scatterer. Gans (1912) finds the induced field in a spheroid to be related to the incident field E_0 as

$$E_\xi = \frac{E_0 \xi}{1 + \frac{m^2/m_0^2 - 1}{4\pi} P} \quad (6-2a)$$

$$E_\eta = \frac{E_0 \eta}{1 + \frac{m^2/m_0^2 - 1}{4\pi} P} \quad (6-2b)$$

$$E_{\zeta} = \frac{E_{o\zeta}}{1 + \frac{m_o^2/m^2 - 1}{4\pi} P'} \quad (6-2c)$$

where ξ is the direction of the axis of rotation (or figure axis) of the ellipse and η and ζ are the directions of two orthogonal diameters. Therefore, from Eq. (6-1),

$$f_{\xi} = (4\pi)^{-1} m_o^2 g E_{o\xi}, \quad f_{\eta} = (4\pi)^{-1} m_o^2 g' E_{o\eta}, \quad f_{\zeta} = (4\pi)^{-1} m_o^2 g' E_{o\zeta} \quad (6-3)$$

where g is the complex quantity

$$g, g' = \frac{V[(m/m_o)^2 - 1]}{4\pi + [(m/m_o)^2 - 1]P, P'} \equiv \frac{3V}{4\pi} L, L' e^{-i\chi, \chi'} \quad (6-4)$$

where

$$P' = 2\pi - P/2.$$

The quantities L , L' , χ , χ' , and g , g' are defined by the identities in Eq. (6-4). For an oblate spheroid (flattened at the poles of the major axis) Gans finds

$$P = \frac{4\pi}{e^2} [1 - \left(\frac{1-e^2}{e^2}\right)^{1/2} \arcsin e] \quad (6-5a)$$

and for a prolate spheroid

$$P = 4\pi \frac{1-e^2}{e^2} \left[\frac{1}{2e} - \ln \left(\frac{1+e}{1-e} \right) - 1 \right] \quad (6-5b)$$

here $e = (a^2 - b^2)^{1/2}/a$ is the eccentricity and a and b are the semi axes of the elliptical cross-section.

The scattered field E_s at distance r from a dipole of moment f is given by

$$E_s = \frac{k_s^2 f}{m_0^2 r} \exp(-i k_s \cdot \vec{r}) \quad (6-6)$$

where $k_s = 2\pi/\lambda$. The r.f. phase factor, $\exp(-i k_s \cdot \vec{r})$, will be neglected because we are interested in the signal magnitude. Also, the scattered power P_s at r is related to the incident power P_o as

$$P_s = \frac{P_o \sigma}{4\pi r^2} \quad (6-7)$$

where σ is the equivalent cross-section of a target isotropically scattering the same power in the direction \vec{r} as the real scatterer. Noting that $P_o, P_s \propto E_o^2, E_s^2$ and that $V = \frac{\pi}{6} D^3$ is the volume of the equivalent sphere; Eqs. (6-3), (6-6), and (6-7) give

$$\sigma_i, \sigma_i' = \left(\frac{4\pi}{3}\right)^2 \frac{\pi^5 D_e^6 (m^2 - 1)^2}{\lambda^4 [4\pi + (m^2 - 1)p, p']^2} = \frac{64\pi^5}{\lambda^4} D_e^6 S, S' \quad (6-8)$$

where σ_i is the cross-section of an individual drop scattering parallel to the principle axis and σ_i' is the scattering cross-section for the two remaining orthogonal axes, and D_e is the diameter of a sphere of equal volume. If we examine the limiting case as $e \rightarrow 0$, and expand both the arc sin factor and the radical in Eq. (6-5a) for small e , it is

found that $P \rightarrow P' \rightarrow 4\pi/3$ so that

$$\sigma_i = \frac{\pi^5}{\lambda^4} D^6 \frac{|\mathbf{m}^2 - 1|^2}{(\mathbf{m}^2 + 2)^2} = \frac{\pi^5}{\lambda^4} D^6 |\mathbf{k}|^2 \quad (6-9)$$

in agreement with the well known result for Rayleigh scattering from small spherical particles (e.g., Battan, 1973).

Of course, Eqs. (6-8) and (6-9) give the scattering cross-section for a single particle only. The total scattered power is therefore proportional to $\sigma = \sum_{vol} \sigma_i$ where the summation is over a volume presumed to be uniformly filled with scatterers. If the size distribution of particles is described by N_D where N_D is the number of drops in the size interval D to $D + dD$, Eq. (6-9) gives

$$\sigma = \frac{\pi^5}{\lambda^4} |\mathbf{k}|^2 \int_0^\infty D^6 N_D dD \quad (6-10)$$

over the whole size range of spherical particles and for spheroidal particles in general Eq. (6-8) gives

$$\sigma, \sigma' = \left(\frac{4\pi}{3}\right)^2 \frac{\pi^5}{\lambda^4} \int_0^\infty \frac{(\mathbf{m}^2 - 1)^2}{[4\pi + (\mathbf{m}^2 - 1)P, P']^2} D^6 N_D dD \quad (6-11a)$$

and therefore from the definitions in Eq. (6-4)

$$\sigma, \sigma' = \frac{\pi^5}{\lambda^4} \int_0^\infty L, L' e^{-iX, X'} D^6 N_D dD \quad (6-11b)$$

Seliga and Bringi (1976) define the quantity

$$Z_{DR} = 10 \log (\sigma/\sigma')$$

as the "differential reflectivity" where σ , σ' are given by Eqs. (6-11a) and (6-11b), and N_D is assumed to obey a Marshall-Palmer distribution, i.e., $N_D = N_0 e^{-3.67/D_0}$. Some insight is provided by first assuming a uniform size distribution and assuming that all particles are oblate spheroids with vertical axes, equal eccentricity and equal volume. Then Eq. (6-8) gives

$$\sigma/\sigma' = g^2/g'^2$$

Geometry of scattering

We first consider the radar backscatter problem, then generalize it to the case of forward scatter because of the interest in scattering on earth-satellite paths. The orientation of the axis of symmetry (figure axis) of the ellipsoid is in the direction ξ and two orthogonal minor axes are chosen in the directions η and ζ . The geometry assumed is shown in Figure 6-2 and is summarized as follows:

- a) choose ξ to be the direction of the rotational or figure axis of the ellipsoid,
- b) choose z to be the propagation direction of both the incident and radar backscattered (with opposite sense) energy,
- c) choose the x axis to be in the direction of the incident field E_0 where the zero subscript is dropped from now on.
- d) without loss in generality, choose one minor axis E_ζ of the ellipsoid to lie in the xy plane (i.e., $\phi' = \phi + 90^\circ$) and the other to lie in the ξz plane (i.e., $\phi' = \phi$, $\delta' = \delta - 90^\circ$).

e) make θ and δ the angles between the ζ direction and the x and z axes respectively. ϕ is the angle between x and the direction of E_ζ projected onto the xy plane. θ' and δ' are the angles between the η direction and the y and z axes respectively, and ϕ' and ϕ'' are the angles between x and the azimuthal directions of E_η and E_ζ .

Dropping the zero subscript the projections of \tilde{E} onto the three axial directions are

$$E_\xi = E \cos\theta = E\ell, \quad E_\eta = E \cos\theta' = Em, \quad E_\zeta = E \cos\phi'' = En$$

and the projections on x are

$$E_{x\xi} = E_\xi \cos\theta = E_\xi \sin\delta \cos\phi, \quad E_{x\eta} = E_\eta \cos\theta' = E_\eta \cos\delta \cos\phi, \quad E_{x\zeta} = -E_\zeta \sin\phi.$$

Similarly, on y and z ,

$$\begin{array}{lll} E_{y\xi} = E_\xi \sin\delta \sin\phi & E_{y\eta} = E_\eta \cos\delta \sin\phi & E_{y\zeta} = E_\zeta \cos\phi \\ E_{z\xi} = E_\xi \cos\delta & E_{z\eta} = -E_\eta \sin\delta & E_{z\zeta} = 0 \end{array}$$

so

$$\begin{array}{lll} E_{x\xi} = E \sin^2\delta \cos^2\phi & E_{x\eta} = E \cos^2\delta \cos^2\phi & E_{x\zeta} = E \sin^2\phi \\ E_{y\xi} = E \sin^2\delta \cos\phi \sin\phi & E_{y\eta} = E \cos^2\delta \cos\phi \sin\phi & E_{y\zeta} = -E \sin\phi \cos\phi \\ E_{z\xi} = E \sin\delta \cos\delta \cos\phi & E_{z\eta} = -E \cos\delta \cos\phi \sin\delta & E_{z\zeta} = 0 \end{array} \quad (6-12)$$

and

$$f_{x\xi} = m_0^2 g E_{x\xi} = CL e^{-i\chi} E_{x\xi}, \quad f_{x\eta} = m_0^2 g' E_{x\eta} = CL' e^{-i\chi'} E_{x\eta},$$

$$f_{x\zeta} = m_0^2 g' E_{x\zeta} = CL' e^{-i\chi'} E_{x\zeta} \text{ etc.}$$

where $C = 3 m_0^2 V / 4\pi$ and V is the volume of the scatterer. Summing all components along x , y , and z ,

$$\begin{aligned} f_x &= CE (Le^{-i\chi} \sin^2 \delta \cos^2 \phi + L'e^{-i\chi'} \cos^2 \delta \cos^2 \phi + L'e^{-i\chi'} \sin^2 \phi) \\ &= CE \left\{ (Le^{-i\chi} - L'e^{-i\chi'}) \ell_1^2 + L'e^{-i\chi'} \right\} \end{aligned} \quad (6-13a)$$

$$\begin{aligned} f_y &= CE \left\{ Le^{-i\chi} \sin^2 \delta \sin \phi \cos \phi + L'e^{-i\chi'} \cos^2 \delta \sin \phi \cos \phi - L'e^{-i\chi'} \sin \phi \cos \phi \right\} \\ &= CE \left\{ (Le^{-i\chi} - L'e^{-i\chi'}) \ell_1 \ell_2 \right\} \end{aligned} \quad (6-13b)$$

$$f_z = CE \cos \phi \cos \delta \sin \delta (Le^{-i\chi} - L'e^{-i\chi'}) = CE (Le^{-i\chi} - L'e^{-i\chi'}) \ell_1 \ell_3 \quad (6-13c)$$

where $\ell_1 = \sin \delta \cos \phi$, $\ell_2 = \sin \delta \sin \phi$, $\ell_3 = \cos \delta$ are the direction cosines of E_ξ projected onto the x , y , and z axis respectively.

If z is chosen to be the propagation direction, $E_z = f_z = 0$. If the E vector lies on the x axis, the propagation plane is yz , and if the x axis is horizontal the radiation is horizontally polarized. If xz is the propagation plane, containing the E vector, the radar is vertically polarized. In either case, f_y is the cross-polarized component of the radiation.

Of course, in reality we are not dealing with single scatterers but with ensembles of scatterers oriented in some manner only describable statistically. Atlas, Kerker, and Hitchfeld suggest three cases of particular interest: (a) the case of random orientation, (b) the case uniform orientation of oblate spheroids with figure axes vertical, and (c) the case of prolates with their major axis arbitrarily oriented in the horizontal plane.

From Eqs. (6-13a,b)

$$f_x^2 = C^2 E^2 \left\{ \ell_1^4 L^2 e^{-2i\chi} + (1 - 2\ell_1^2 + \ell_1^4) (L')^2 e^{-2i\chi} + (\ell_1^2 - \ell_1^4) LL' e^{-i(\chi+\chi')} \right\} \quad (6-14a)$$

$$f_y^2 = C^2 E^2 (\ell_1 \ell_2)^2 \left\{ L^2 e^{-2i\chi} - 2LL' e^{-i(\chi+\chi')} + (L')^2 e^{-2i\chi'} \right\} \quad (6-14b)$$

If an average is taken over a complete cycle of the incident wave propagating such that $L \exp(-i\chi)$, $L' \exp(-i\chi') \propto \exp i(\omega t - k_0 z - \chi, \chi')$

$$\overline{f_x^2} = \frac{C^2 E^2}{2} \left\{ \overline{\ell_1^4} |L|^2 + (1 - 2\overline{\ell_1^2} + \overline{\ell_1^4}) |L'|^2 + 2(\overline{\ell_1^2} - \overline{\ell_1^4}) |L| |L'| e^{-i(\chi-\chi')} \right\} \quad (6-15a)$$

$$\overline{f_y^2} = \frac{C^2 E^2}{2} \overline{(\ell_1 \ell_2)^2} \left\{ |L|^2 - 2|L| |L'| e^{-i(\chi-\chi')} + |L'|^2 \right\} \quad (6-15b)$$

Perfect sphere

Return to Eqns. (6-4) and (6-5) and consider their limiting form for a perfect sphere. Note that $e = 0$ for a sphere. If the \sin^{-1} factor and the radical in Eq. (6-5a) are expanded in series for small e , it is found that $P = P' \rightarrow 4\pi/3$ as $e \rightarrow 0$ so that

$$g = g' = \frac{3V}{4\pi} \frac{(m^2 - 1)}{(m^2 + 2)} = a^3 \frac{|m^2 - 1|}{(m^2 + 2)} \equiv a^3 K \quad (6-16a)$$

for a sphere, i.e., $L e^{-i\chi} = K$. Noting that $\ell_1 = \ell_2 = 0$ if we choose a coordinate system for the sphere such that $\xi = z$, Eq. (6-14a) gives

$$f^2 = m_o^4 a^6 K^2 E^2 \equiv (3/4\pi)^2 m_o^4 V^2 K^2 E^2 \quad (6-16b)$$

in agreement with the classical result for the dipole moment of a sphere.

Random Orientation

If the orientation of the axis is entirely random

$$\overline{\ell_1^2} = \frac{1}{2} \int_{-1}^1 \ell_1^2 d\ell_1 = \frac{1}{3}, \overline{\ell_1^4} = \frac{1}{2} \int_{-1}^1 \ell_1^4 d\ell_1 = \frac{1}{5} \text{ etc.}$$

Then

$$\overline{f_x^2} = \frac{C^2 E^2}{2} \left\{ \frac{1}{5} |L|^2 + \frac{8}{15} |L'|^2 + \frac{4}{15} |L||L'| \cos(\chi - \chi') \right\} \quad (6-17a)$$

$$\overline{f_y^2} = \frac{C^2 E^2}{2} \cdot \frac{1}{15} \left\{ |L|^2 - 2|L||L'| \cos(\chi - \chi') + |L'|^2 \right\} \quad (6-17b)$$

Oblate Spheroids

Suppose the scatterers are all oblate spheroids, oriented with their figure axes vertical. The vertical direction is then ξ . Also, choose the x axis to be horizontal. Since z is by definition the propagation direction, the propagation plane is then zy ; it must contain E_ξ (i.e., $\theta = 90^\circ$) if ξ is to be vertical and x horizontal. Therefore, the projection of E_ξ on x , is $\ell_1 = 0$ and on y is $\ell_2 = \sin \delta$.

Note that the polarization has not been specified. The Eqns. (6-15a) and (6-15b) were developed assuming \tilde{E} to be horizontal, lying along x . For vertical polarization the x and y axes can be exchanged. Then f_x and f_y must be interchanged and also ℓ_1 and ℓ_2 .

Thus for horizontal polarization

$$\overline{f_x^2} = \frac{C^2 E^2}{2} |L'|^2 \quad (6-18a)$$

$$\overline{f_y^2} = 0 \quad (6-18b)$$

and for vertical polarization

$$\overline{f_x^2} = 0 \quad (6-19a)$$

$$\begin{aligned} \overline{f_y^2} &= \frac{C^2 E^2}{2} \left\{ |L|^2 \sin^4 \delta + |L'|^2 (1 - 2 \sin^2 \delta + \sin^4 \delta) \right. \\ &\quad \left. + 2 |L| |L'| (\sin^2 \delta - \sin^4 \delta) \cos(\chi - \chi') \right\}. \end{aligned} \quad (6-19b)$$

Thus with horizontal polarization the \tilde{E} vector is perpendicular to the y , z , and ξ axes, so only f_x^2 is non zero. Furthermore, since the x axis of the spheroid is independent of δ , the moment f_x does not depend on elevation angle. When the propagation plane $y\xi$ contains the \tilde{E} vector, the polarization is said to be vertical. The projection of \tilde{E} onto the x axis is then zero so $f_x = 0$, but the projection onto ξ clearly depends on the angle between ξ and the propagation direction z , so f_y depends strongly on δ .

Prolate Spheroids

Suppose the scatterers are prolate spheroids with their major axis lying in the horizontal plane. Then ξ is horizontal as is x by assumption.

Therefore the horizontal plane is $x\xi$ and ℓ_1 , the projection of E_ξ onto x , is just $\ell_1 = \cos\theta$, and ℓ_2 , the projection of E_ξ onto y , is $\ell_2 = \sin\theta \sin\delta$.

Thus

$$\overline{\ell_1^2} = \frac{1}{2}, \quad \overline{\ell_2^2} = \frac{\sin^2\delta}{2\pi} \int_{-\pi}^{\pi} \sin^2\theta d\theta = \frac{\sin^2\delta}{2}$$

$$\overline{\ell_1^4} = \frac{3}{8}, \quad \overline{(\ell_1 \ell_2)^2} = \frac{\sin^2\delta}{2\pi} \int_{-\pi}^{\pi} \cos^2\theta \sin^2\theta d\theta = \frac{1}{8} \sin^2\delta$$

$$\overline{\ell_2^4} = \frac{3}{8} \sin^4\delta;$$

so for horizontal polarization and horizontal prolates,

$$\overline{f_x^2} = \frac{C^2 E^2}{2} - \frac{3}{8} |L|^2 + \frac{1}{4} |L| |L'| \cos(\chi - \chi') + \frac{3}{8} |L'|^2 \quad (6-20a)$$

$$\overline{f_y^2} = \frac{C^2 E^2}{2} - \frac{1}{8} \sin^2\delta |L|^2 - 2 |L| |L'| \cos(\chi - \chi') + |L'|^2 \quad (6-20b)$$

and for vertical polarization and horizontal prolates

$$\overline{f_x^2} = \frac{C^2 E^2}{2} - \frac{1}{8} \sin^2\delta |L|^2 - 2 |L| |L'| \cos(\chi - \chi') + |L'|^2 \quad (6-21a)$$

$$\begin{aligned} \overline{f_y^2} = & \frac{C^2 E^2}{2} - \frac{3}{8} |L|^2 \sin^4\delta + (\sin^2\delta - \frac{3}{4} \sin^4\delta) |L| |L'| \cos(\chi - \chi') \\ & + (1 - \sin^2\delta + \frac{3}{8} \sin^4\delta) |L'|^2. \end{aligned} \quad (6-21b)$$

Differential reflectivity from non-spherical particles

Suppose a volume containing oblate spheroidal scatterers of common size and shape is viewed simultaneously by radars of horizontal and vertical polarization. Furthermore, assume that the axes of rotation of the spheroids are all vertical. Then the ratio of powers in the two polarizations will be given by the ratio of Eqs. (6-17a) and (6-18b). The ratio will in generally vary dramatically with zenith angle. Examples are shown in Figs. 6-9 thru 6-12 parametric in the ratio a/b where a is the semi axis of rotation (principle axis) and b is the orthogonal semi axial dimension. However, if the two radars are viewing the volume horizontally ($\delta = 90^\circ$) a rather simple relationship is obtained as shown in Figs. 6-3 and 6-4. For either water or ice the ratio of the powers in the two polarizations depends mainly on the ratio a/b with only a weak dependence on radar wavelength λ or temperature. Therefore, a simple measure of power backscattered on the two polarizations provides a direct measure of drop shape.

In order to obtain information on actual drop-size, it is necessary to use either a relationship between absolute reflectivity and drop size or a relationship between drop shape and drop size. The latter relationship has been investigated by Pruppacher and Beard (1970). They studied water drops falling at terminal velocity in a wind tunnel at 20° C at a pressure of sea level in a nearly saturated environment. They obtained drop-shape photographically, and examples of various size drops are shown in Figs. 6-5 and 6-6. At first glance the drops in Fig. 6-5, which are between 30 and 450 μm radii appear to be spherical. However, with magnification even drops as small as 155.5 μm radius were found to be deformed. In summary, drops less

than about 140 μm (Reynold's No ≈ 20) showed no deformation; drops such that $140 \mu\text{m} \leq a \leq 500 \mu\text{m}$ were slightly, but measurably, deformed oblates conforming fairly well to the relations obtained by Imai (1950) which can be combined (Pruppacher and Beard) into the expression

$$a/b = [1 - (9/16) a_0 \rho v_t^2 / s]^{1/2} \quad (6-22)$$

where a_0 is drop radius, in cm, ρ is saturated air density ($1.19 \times 10^{-3} \text{ g cm}^{-3}$), v_t is terminal fall velocity in cm s^{-1} , and s the surface tension of water at 20° C ($\approx 72.75 \text{ erg cm}^{-2}$).

Figure 6-6 shows drops in the size range $0.5 \leq a_0 \leq 4.5 \text{ mm}$. It shows that the shape deviates markedly from spherical in this range, but up to 1.5 mm radius the shape is still well approximated by an oblate spheroid. At larger sizes the bottom of the drop is flattened. The various experimental results to be found in the literature were collected by Pruppacher and Beard and are summarized in Fig. 6-7. In the size range $0.5 \leq a_0 \leq 4.5 \text{ mm}$ the deformation a/b is linearly related to size a_0 by the empirical expression

$$a/b = 1.030 - 0.124 a_0 \quad (6-23)$$

where a_0 is in mm.

Pruppacher and Pitter (1971) have presented a method with more physical basis for calculating drop shape but the method requires assumptions about the appropriate pressure distribution over the drop and needs a high speed computer. From the radar-observed deformations a/b it is easy to calculate

effective values of drop radius a_o using Eqs. (6-22) and (6-23). Then, using empirical fall velocity-size relations given by Gunn and Kinzer (1949) or by Foote and DuToit (1969), the fall velocity in quiet air can be retrieved. Finally, with Doppler observation of total fall velocity, the contribution from vertical air motion can in principle be deduced.

The discussion above has been based on the assumption that all drops in the volume are of the same size and shape. Seliga and Bringi (1976) adopt the more reasonable assumption that the drop sizes form a Marshall-Palmer number distribution $N_D = N_o \exp(-\Lambda D_e)$. The total backscattered power

$$P \propto \int_{D=0}^{\infty} \sigma_D N_D dD_e$$

where the index "e" refers to a sphere of equal volume. So from Eq. (6-10),

$$\frac{\sigma'}{\sigma} = \frac{\int_0^{\infty} D_e^6 S_i' N_D dD_e}{\int_0^{\infty} D_e^6 S_i N_D dD_e} = \frac{Z'}{Z} \quad (6-24)$$

where S, S' are defined by the identity, Eq. (6-8). Bringi and Seliga (1976) call $10 \log (Z'/Z)$ the "differential reflectivity" = Z_{DR} although "differential dBZ" would be a more appropriate term, as Z is conventionally called reflectivity factor to distinguish it from the reflectivity η . In their interpretation Z' is the value for horizontally polarized incident radiation and Z is that for the vertically polarized wave. When the distribution for N_D is inserted in Eq. (6-24), N_o cancels and D_e disappears in the integration. Therefore, since the mass median diameter $D_o = 3.67/\Lambda$, the quantity D_o is uniquely determined by the radar power measurement Z_H/Z_V . Then, from an absolute measurement of either Z_H

or Z_V , the value of N_o can be found. Using Pruppacher and Beard results to relate a/b to D_e and thus calculate P , P' and S , S' ; Seliga and Bringi compute the integrals in Eq. (6-24) by numerical methods and obtain the results shown in Fig. 6-8 (solid curves) where Z_{DR} is defined above and where N_o is related to the horizontal polarization reflectivity factor through the quantity $10 \log (Z_H/N_o)$.

It is noteworthy that essentially the same relationship between Z_{DR} and size scale is found from Eqs. (6-18a) and (6-19b) by suitable definition of the size scale (say D_1) to use in the uniform size model assumed in the use of (6-18a) and (6-19b). The dashed curve shown in Fig. 6-8 for Z_{DR} is found if the abscissa is D_1 instead of the mass median diameter D_o , where $\Delta D_1 = 2.0$. (Note that $\Delta D_o = 3.67$.) Thus, defining $D_1 = 0.54D_o$, the rather simple reasoning that led to Figs. 6-4 and 6-5 can be used to deduce the drop-size scale D_o from the differential reflectivity, effectively by-passing the numerical integration of Seliga and Bringi and the shape-scale-fall velocity relations of Pruppacher and Beard.

Attenuation by non-spherical particles

The total attenuation, Q_t , of radar waves by small particles is made up of attenuation due to the scattering of energy out of the beam, Q_s , and of attenuation due to absorption Q_a . That is, $Q_t = Q_s + Q_a$. In the Rayleigh approximation for very small spherical particles (e.g., see Battan, 1973)

$$Q_s = \frac{128}{3} \cdot \frac{\pi^5 a^6}{\lambda^4} \cdot \left| \frac{m^2 - 1}{m^2 + 2} \right|^2 = \frac{24\pi^3}{\lambda^2} \cdot \left(\frac{V}{\lambda} \right)^2 |K|^2 \quad (6-25)$$

$$Q_a = \frac{8\pi^2 a^3}{\lambda} \operatorname{Im} \left(-\frac{m^2 - 1}{m^2 + 2} \right) = 6\pi \left(\frac{V}{\lambda} \right) I(-K) \quad (6-26)$$

In order to generalize these results to the case of non-spherical particles return to Eqs. (6-4) and (6-5a,b) and consider their limiting form for the case of a perfect sphere. In Eq. 6-5a) if the \sin^{-1} factor and the radical are expanded in series for small e , it is found that $P \rightarrow 4\pi/3$ as $e \rightarrow 0$ and Eq. (6-16a) is obtained. Eqs. (6-21) and (6-22) can then be written

$$Q_s = \frac{8\pi}{3m_0} \left(\frac{2\pi}{\lambda} \right)^4 |g|^2$$

$$Q_a = \frac{8\pi^2}{\lambda m_0} \operatorname{Im}(-g)$$

Generalizing to the case of spheroids of random orientation

$$Q_s = \frac{8\pi}{9m_0} \left(\frac{2\pi}{\lambda} \right)^4 (|g|^2 + 2|g'|^2) \quad (6-27)$$

$$Q_a = \frac{8\pi^2}{3\lambda m_0} \operatorname{Im}(-g - 2g') . \quad (6-28)$$

We see from Eqs. (6-25) and (6-26) that $Q_s \propto (V/\lambda)^2$, whereas $Q_a \propto V/\lambda$. Therefore, when considering liquid cloud droplets and cm or mm radar wavelengths, Q_a should easily dominate Q_s because of the relatively small volume of each cloud droplet. However, the imaginary part of the refractive index of ice is

very small, i.e., $m \approx 1.78 - i2.89 \times 10^{-4}$ at -10°C , whereas for liquid water $m \approx 7.14 - i2.89$ at 0°C for a 3.2 cm wavelength radar (Battan, 1973). Obviously Eq. (6-27) can be used to calculate the attenuation in water clouds, but for ice particles the scattering cross-section is the important component and Eq. (6-28) must be used.

Scattering in an arbitrary direction

We have so far considered only backscatter because that is the case of most interest in radar. However, in bistatic radar systems or in analysis of the effect of spheroidal scatterers on oneway communications and telemetry paths it is necessary to generalize the previous expressions.

If the scatterers are not spherical, the scattered electric field may have components E_x , E_y , and E_z in all coordinate directions even though the incident field is assumed to propagate in the z direction. The dipole moments f_x , f_y , and f_z may exist along all three axes as shown in Figure 6-13. We consider the scattering at an angle γ with the z axis and let the angle γ lie in the xz plane. The total electric field associated with the wave scattered at the angle γ is therefore the vector sum of the y component and the components of E_x and E_z projected onto AB, the normal to the propagation direction in the xz plane. The scattered field has dipole moments f_x , f_y , and f_z , and the intensity of the power radiated is

$$I(\gamma) = (2\pi/\lambda)^4 (f_y^2 + f_x^2 \cos^2 \gamma + f_z^2 \sin^2 \gamma) \quad (6-29a)$$

In the backscatter direction, for which $\gamma = 180^\circ$, this reduces to simply

$$I(\gamma) = (2\pi/\lambda)^4 (f_y^2 + f_x^2) \quad (6-29b)$$

as is to be expected.

Polarization effects in the forward scatter direction have recently assumed great importance. The depolarization that results from non-spherical scatterers imposes a major limitation on the possible use of polarization diversity as a means of increasing channels on satellite-to-earth paths. It is readily seen from the above, that both attenuation and depolarization are simply calculated within the approximations contained in the Gans theory. If the (spheroidal) shape of the scatterers is known; the depolarization and the attenuation are intimately linked through Gans' factor g .

Imagine, then, the surprise of experimentalists when the phenomenon of "anomalous depolarization" without attenuation was discovered on satellite to earth paths.

The answer, of course, is to be found in the comparison of Eqs. (6-14), (6-15), and (6-19). If we consider ice needles, it is immediately clear from Eq. (6-14b) and (6-15a) that there will be significant cross-polarized scatter from ice prolates unless $\delta = 0$. On the other hand the imaginary part of the refractive index of ice is very small ($k \approx 8 \times 10^{-4}$) so Eq. (6-19) will yield very small attenuation. It seems clear (Cox et al., 1976) that the depolarization results from ice particles in the atmosphere.

Conclusions and possible observational applications

- 1) When the incident electric vector is perpendicular to a plane containing one of the spheroid axes, there is no dipole moment excited along that axis so there will be no cross polarized component.

- 2) Ice spheroids are relatively weak backscatterers compared with water spheroids of comparable volume, and their backscatter and attenuation depends only weakly on shape. On the other hand, water spheroids are very shape-dependent. It is pointed out by Atlas, Kerker, and Hitchfeld, (1953), that the shape effect should be completely negligible for snow. They base their conclusions on the fact that $(m^2 - 1)/(m^2 + 2) \propto \rho$ where ρ is density, and note that P is proportional to $m^2 - 1$. Since the density of ice is about 0.9 and that of snow about on the order of magnitude less, the very weak shape dependence of pure ice is further greatly reduced when it occurs in the form of snow. However, for melting snow, when the flakes are water coated, the reflectivity might become very shape-dependent.
- 3) Kerker, Langleben, and Gunn (1951) and Warner (1977) have made computations on the basis of theory assuming an ice sphere to be surrounded by a thin water film. They find that even a very thin water coating is sufficient to make the scatterer behave like a water droplet of the same mass.
- 4) For oblates the backscattered power doesn't change with δ for horizontal polarization, but for vertically polarized transmission the backscattered (parallel polarized) power decreases dramatically as δ increases. Thus the ratio of the two powers (difference in dB) is a measure of scatterer shape if an RHI scan is used. This is also true if prolates (needles) have their major axis horizontal but are randomly oriented in azimuth.
- 5) For prolate spheroids whose principal axes are vertical, the backscatter increases as the zenith angle δ increases.
- 6) The ratio of the backscattered power in vertical and horizontal polarization and their phase difference is a sensitive measure of drop-shape. If both radars view the volume at horizontal grazing angle ($\delta = 90^\circ$) especially

simple relations are found as seen in Figs. 6-3 and 6-4. The ice phase differs greatly from the water phase. Drop shape a/b is closely related to drop-size so the dual polarization measurement is of significant potential value to the meteorologist monitoring locally changing conditions. The drop-shape deviates significantly from spherical only for drops greater than about 200 microns, so such a measurement may not be of much use in studies of non-precipitating clouds. However, it should be a sensitive indicator of when the first few large drops appear and permit the observer to monitor the occurrence and growth rate of precipitation-size particles within clouds.

7) Polarization measurements can reveal to the meteorologist much about conditions near the freezing level by exploiting the bright-band phenomenon. As pointed out above, the reflectivity of snow above the freezing level should be very small and independent of polarization at all zenith angles δ . However, a region of high reflectivity occurs just below the zero degree isotherm. Suggested reasons for the enhanced reflectivity producing the bright band include (1) transition from ice to water (Austin and Bemis, 1950) and (2) change in shape as particles melt (Wexler, 1955). Based on depolarization measurements, Wexler concluded that shape changes accounted for only about 1.5 dB of enhancement. Because flat oblates with vertical axes would not be expected to produce depolarization, but should produce significant aspect vs. reflectivity changes, an experiment should be done using two polarizations and measuring the relative backscatter dependence on elevation angle in an RHI scan. However, horizontally oriented prolates (or needles) could cause significant depolarization, so measurements of both the co-polarized and cross-polarized backscatter on both polarizations would be of value to the meteorologist wishing to monitor the change of

state and distribution of particles in his vicinity. The dependence of the ratio of backscattered power in the vertical and horizontal polarizations on zenith angle δ and on wavelength λ is shown in Figs. 6-9 thru 6-12.

8) For ice, k (the imaginary part of the refractive index) is very small so χ is small and attenuation due to absorption is very small. Attenuation is almost entirely due to scattering.

9) Equations (6-18b) and (6-19a) show that no cross-polarization results from oblate spheroids whose axes are vertical for either horizontal or vertical polarization.

10) Prolate spheroids whose major axes are randomly oriented in horizontal planes produce significant cross polarization of the backscattered signal.

11) When the electric vector is parallel to a plane containing the major or minor axis of the spheroid only the dipole moment along that axis is excited.

12) By monitoring the height region containing the freezing level, the meteorologist could tell when an ice cloud begins to precipitate, because the bright-band phenomenon depends on particles falling through the freezing level. In fact the distinctive banding is partly a result of the change in particle fall velocity as they change state from snow to liquid (see Figure 6-14, taken from Lhermitte and Atlas, 1963). In Fig. 6-14 the radar was of wavelength $\lambda = 3.2$ cm and pointing vertically. The bright-band is often more intense than would be expected simply from the change in state from ice to snow. Note that Z_e increased by a factor of 30.6 between level 2 and level 3 in Figure 6-14. Referring to Eq. (6-9) and noting that $|k|^2 \approx 0.92$ for water and $|k|^2 \approx 0.197$ for ice, we see that the change from ice to liquid can

only account for a factor of about 5. This fact caused Lhermitte and Atlas (1963) to propose that rapid aggregation of ice crystals into larger and larger snowflakes proceeded down to level 3 within the bright-band. However, an alternate explanation may be found in Figure 6-15, which shows the ratio of backscattered power from water and ice particles. It shows that the backscattered power increases by a factor of 41 if the scattering particle changes from an ice oblate of axial ratio 0.1 (perhaps a snowflake) to a liquid water oblate (as the snowflake melts).

Likewise, Lhermitte and Atlas point out that the increase in fall speed of the liquid rain can only account for about one-third of the observed decrease in reflectivity, below the melting layer and they suggest that drop break-up, in which each drop divides into 4-6 drops, must be occurring. However, if the backscatter from an oblate (water coated) ice particle is compared with a spherical water drop it is found that the latter is greater by a factor of about 17 - again in good agreement with the observed difference between levels 3 and 4.

These rough calculations assume equal volumes and densities for the different particles - an assumption which cannot be easily justified, but they indicate the potential importance of particle shape and suggest that the subject of bright-band formation and morphology is not closed. Since aggregation is an important mechanism of particle growth, and particle break-up is an important control on drop-size, the proper interpretation of the bright-band is important to the local forecaster.

APPENDIX

The Radar Equation

The power intercepted and reradiated by a target is

$$\frac{P_t G_T A_T}{4\pi r^2} \quad (A1)$$

where P_t is transmitted power, G_T is gain of the transmitting antenna, and A_T is the target cross-sectional area. If the target scatters isotropically, the power intercepted by the receiving antenna is

$$\frac{P_r G_T A_T}{4\pi r^2} \frac{A_e}{4\pi r^2} \quad . \quad (A2)$$

The effective area A_e of the receiving antenna is related to its gain by

$$A_e = G_R \frac{\lambda^2}{4\pi} \quad . \quad (A3)$$

For a parabola whose aperture is A_p

$$G_R \approx A_p \frac{8\pi}{3\lambda^2} \quad \text{so} \quad A_e \approx \frac{2}{3} A_p \quad . \quad (A4)$$

Early derivations of the radar equation assumed the power to be constant between half-power points of the beam and zero elsewhere. For such a "top hat" beam

$$G_R = 16/\theta\phi \quad (A4a)$$

or just $G_R = 16/\theta^2$ if the beam is conical with beamwidth θ (rad). However, Probert-Jones (1962) studied the more realistic case of a Gaussian beam. The gain of such an antenna is related to its beamwidths θ, ϕ in radians, as

$$G_R = k^2 \pi^2 / \theta\phi \quad (A4b)$$

where k^2 is a dimensionless constant near unity depending on how much of the power from a particular antenna feed is intercepted by the dish. If we consider a parabolic dish of diameter D ,

$$\theta = \phi = 1.56 \lambda/D \quad (A5)$$

for a top hat beam, and from Eq. (A4) and Eq. (A4b)

$$\theta = \phi = 1.22 \lambda/D \quad (A5a)$$

for a Gaussian beam.

If we replace the geometrical target cross-sectional area with the backscattering cross-section σ (which is the ratio of the actual backradiated power by the target to the power that would have been backscattered by an isotropic scatter) and replace A_e in Eq. (A2) using Eq. (A3), we find for a top hat beam

$$P_r = P_t \frac{G^2 \sigma \lambda^2}{64\pi^3 r^4} . \quad (A6)$$

Radar Reflectivity and Backscatter

Separating the system parameters from target parameters and range, we can write

$$P_r = \frac{P_t G^2 \lambda^2}{64\pi^3} \frac{\sigma}{r^4} = K \frac{\sigma}{r^4} . \quad (A7)$$

If N is the total number of scatterers in a volume V , the total received power is

$$P_r = \frac{K}{r^4} \sum_{i=1}^N \sigma_i . \quad (A8)$$

If we choose to express the summation in terms of an average reflectivity per unit volume, it can be written

$$P_r = \frac{K}{r^4} \eta V \quad (A9)$$

where V is volume and the quantity

$$\eta = \frac{1}{V} \sum_{i=1}^N \sigma_i \quad (A10)$$

is the so-called radar reflectivity.

If τ is the pulse length, the effective pulse volume for distances much greater than a pulse length is approximately

$$V = \frac{\pi r^2 \theta \phi c \tau}{8} \quad (A11)$$

where θ and ϕ are the radar beamwidths of a top hat beam. Insertion into Eq. (A9) yields, for the top hat beam,

$$P_r = \frac{P_t G^2 \lambda^2}{64\pi^2} \frac{\eta}{r^2} \frac{\theta \phi c \tau}{8} . \quad (A12)$$

For a Gaussian beam the integration over the intercepted volume should include the gain function, so

$$P_r = \frac{P_t \lambda^2}{64\pi^3} \int_V \frac{G^2 \theta \phi \eta}{r^4} dV \quad (A13)$$

which may be integrated to yield (Probert-Jones, 1962)

$$P_r = \underbrace{\frac{c}{1024\pi^2 \ln 2}}_{\text{constant}} \underbrace{(P_t \tau \lambda^2 G_o^2 \theta \phi)}_{\text{radar parameters}} \underbrace{\frac{\eta}{r^2}}_{\text{target parameters}} \quad (A14)$$

where G_o is defined by the following expression for gain with a Gaussian beam:

$$G(\theta, \phi) = G_o \exp - \left[\left(\frac{\theta^2}{2\sigma_\theta^2} + \frac{\phi^2}{2\sigma_\phi^2} \right) \right]$$

Probert-Jones also took account of the fact that when the entire transmitted beam is filled with targets the backscattered beam differs from the transmitted beam pattern. He therefore assumed an equivalent cone and found the power to be reduced by the factor $(2 \ln 2)^{-1}$ which appears in the constant factor of Eq. (A14).

After eliminating G using (A3) and (A4a), Eq. (A12) gives for a "top hat" beam:

$$P_r = 0.0795 P_t A_e \frac{\Delta}{r^2} \eta \quad (A15)$$

where $\Delta = ct/2$ is the range cell depth. From Eqs. (A14), (A3) and A4b we find for a Gaussian beam:

$$P_r = 0.0354 P_t A_e \frac{\Delta}{r^2} \eta . \quad (A15a)$$

We see that calculated received power will be overestimated by 3.5 dB if a "top hat" beam is assumed as was done prior to 1962.

Backscatter from Spherical Drops

For spherical targets σ and η can be related to the refractive index of the particulate (say ice or water). From Mie theory for backscattering from a spherical drop

$$\sigma = \frac{\pi a^2}{\alpha^2} \left| \sum_{j=1}^{\infty} (-1)^j (2j+1) (a_j - b_j) \right|^2 \quad (A16)$$

where

a is drop radius

$$\alpha = 2\pi a/\lambda$$

a_j are the coefficients of terms arising from induced magnetic dipoles, quadrupoles, etc.

b_j are the coefficients of terms arising from induced electric dipoles, quadrupoles, etc.

j number of the term in the expansion.

The coefficients a_j , b_j can be expressed in terms of Bessel and Hankel functions of the 2nd kind with arguments α and refractive index

$$m = n - ik$$

where n is refractive index and k is the absorption coefficient. In the Rayleigh approximation of $a \ll \lambda$

$$\sigma_i = \frac{\lambda^2}{\pi} \alpha^6 \left| \frac{m^2 - 1}{m^2 + 2} \right|^2 = \frac{(2\pi)^6 a^6 \lambda^2}{\lambda^6 \pi} |K|^2 = \frac{2^6 \pi^5 a^6}{\lambda^4} |K|^2 \quad (A17)$$

so

$$\sigma \equiv \sum_i \sigma_i = \frac{\pi^5}{\lambda^4} |K|^2 \sum_i N_i D_i^6 \quad \text{in the Rayleigh limit} \quad (A18)$$

or

$$\sigma = \frac{36\pi^3}{\lambda^4} \frac{|K|^2}{\rho^2} \frac{M^2}{\sum N_i D_i^3} \quad (A19)$$

where $K = |(m^2 - 1)/(m^2 + 2)|$. $|K|^2 \approx 0.93$ for water, D is drop diameter, ρ is density $\approx 1.0 \text{ gm cm}^{-3}$ and $M = (\pi/6) \rho \sum N_i D_i^3$ is the mass of liquid water per unit volume.

Radar reflectivity (Eq. A10) is thus related to the radar reflectivity factor,

$$Z = \sum_i N_i D_i^6 \quad (\text{where the summation is over all size increments in a unit volume}) \quad (\text{A20})$$

as

$$\eta = \frac{\pi^5 |k|^2 Z}{\lambda^4} \quad (\text{A21})$$

so

$$Z = \frac{\lambda^4 \eta}{\pi^5 |k|^2}. \quad (\text{A22})$$

Since the total mass of water in the unit volume is $M = (\pi/6)\rho \sum N_i D_i^3$ we have from (A20)

$$Z = \frac{36M^2}{\rho^2 \pi^2 N} \quad (\text{A23})$$

if the volume is assumed to contain N drops of uniform size \bar{D} so that $Z = N\bar{D}^6$. The reflectivity factor Z is usually expressed in units of (mm^6/m^3) introducing a factor of 10^{18} ; thus from Eqs. (A15) and (A21)

$$Pr = 2.26 \times 10^{-17} \frac{P_t A_e}{\lambda^4} \frac{\Delta}{r^2} Z \quad (\text{top hat beam})$$

and from Eqs. (A15a) and A21)

$$Pr = 1.01 \times 10^{-17} \frac{P_t A_e}{\lambda^4} \frac{\Delta}{r^2} Z. \quad (\text{Gaussian beam})$$

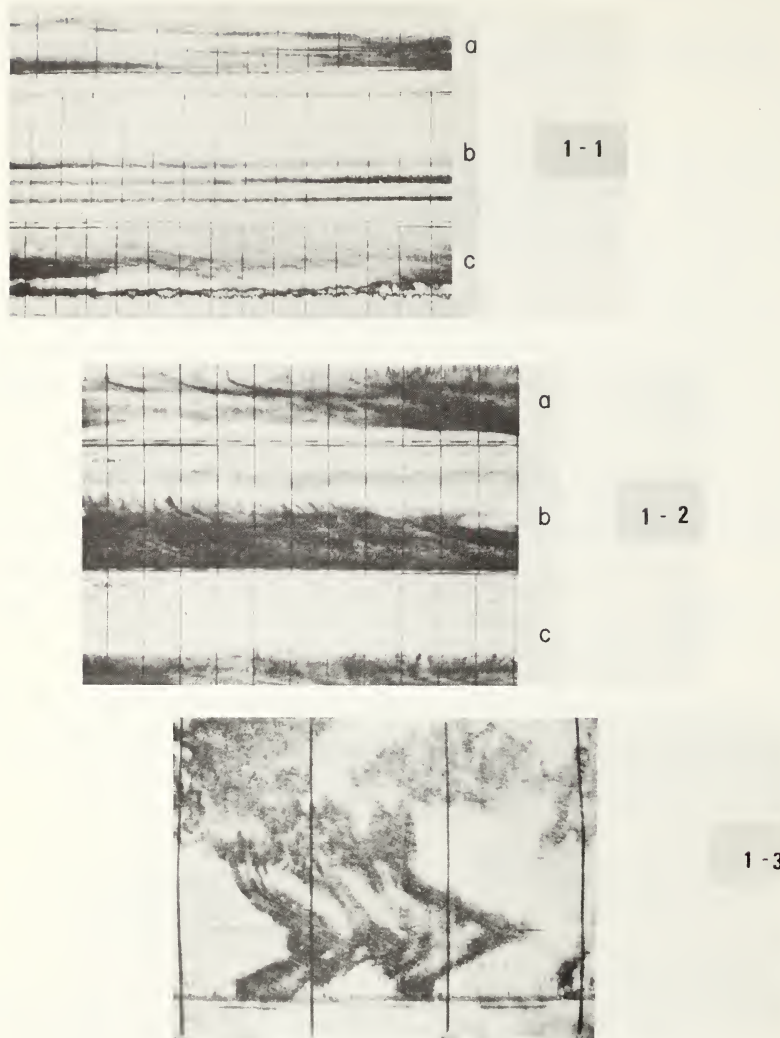


Figure 1-1,2,3. Radar cloud observations obtained with a TPQ-11, 8.6 mm, vertically pointing radar. Figure illustrates temporal changes within cloud structure and the influence of wind shear. (Petrocci and Paulsen, 1972.)

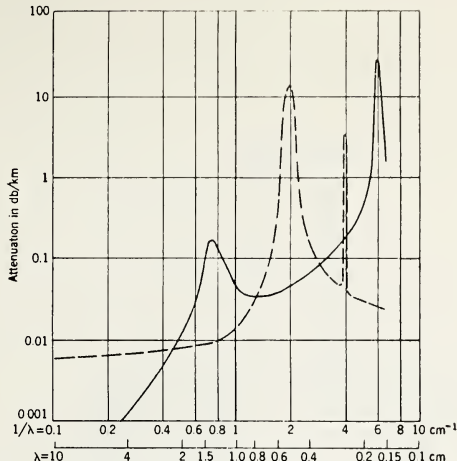


Figure 2-1a. Theoretical values of atmospheric attenuation by oxygen and uncondensed water vapor at sea level for a temperature of 20° C. The solid curve gives the attenuation by water in an atmosphere containing 1 per cent water molecules ($\rho = 7.5 \text{ g/m}^3$) for $\Delta\nu/c = 0.10 \text{ cm}^{-1}$. The dashed curve is the attenuation by oxygen for $\Delta\nu/c = 0.02 \text{ cm}^{-1}$, where $\Delta\nu$ is line width. (From Kerr, 1951).

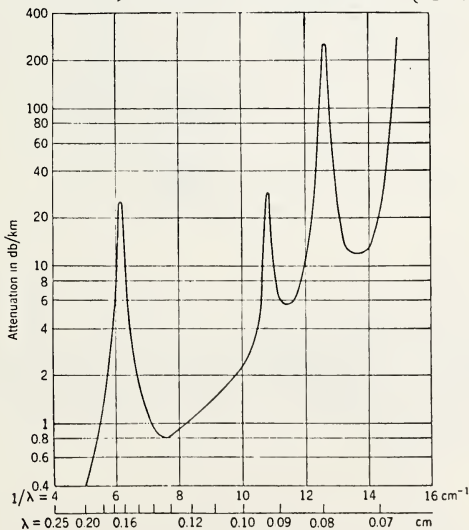


Figure 2-1b. Theoretical values of atmospheric attenuation by uncondensed water vapor in the millimeter region for a temperature of 20°C. The curve is for an atmosphere containing 1 per cent water molecules ($\rho = 7.5 \text{ g/m}^3$) for $\Delta\nu/c = 0.11 \text{ cm}^{-1}$, where $\Delta\nu$ is line width. (From Kerr, 1951).

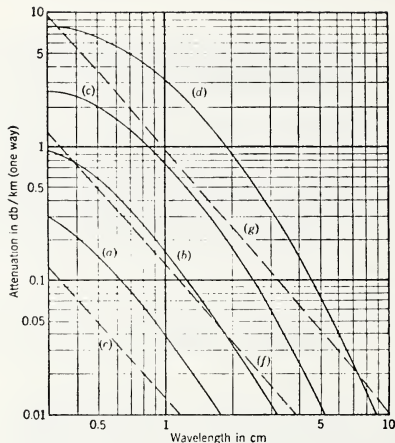


Figure 2-2. Theoretical values of attenuation by rain and fog. Solid curves show attenuation in rain of intensity. (a), 0.25 mm/hr (drizzle); (b), 1 mm/hr (light rain); (c), 4 mm/hr (moderate rain); (d), 16 mm/hr (heavy rain). Dashed curves show attenuation in fog or cloud; (e), 0.032 g/m³ (visibility about 600 m); (f), 0.32 g/m³ (visibility about 120 m); (g), 2.3 g/m³ (visibility about 30 m). (From Kerr, 1951.)

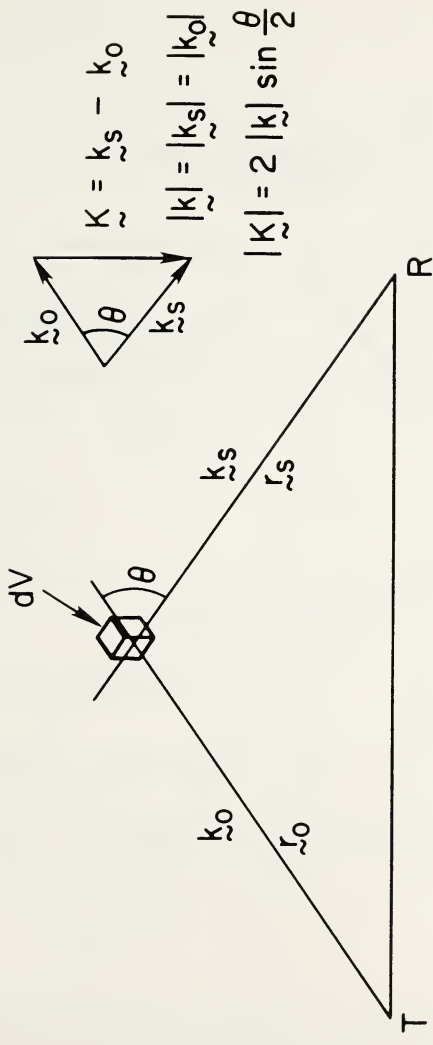


Figure 2-3. Schematic of scattering geometry due to volume element dV between transmitter T and receiver R . Defines the relationship between the various wavenumbers.

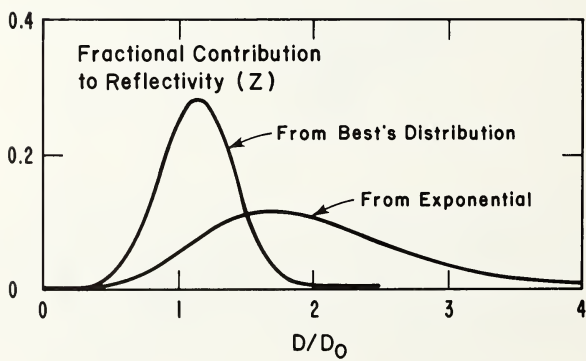
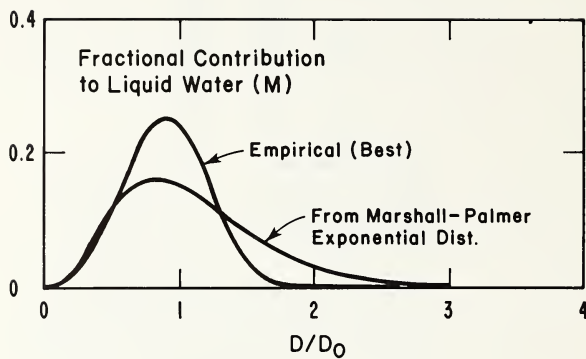


Figure 4-1. Spectrum of fractional contribution to liquid water and fractional contribution to radar reflectivity factor for Best's drop-size distribution and for exponential distribution.

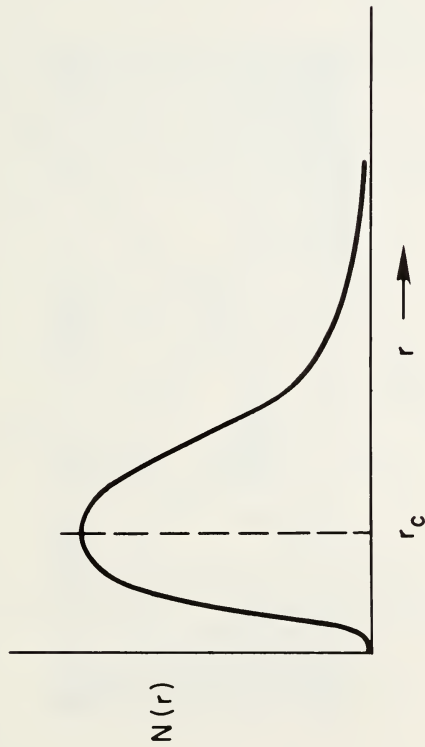


Figure 4-2. Schematic of modified gamma distribution (Beirnendjian, 1969).

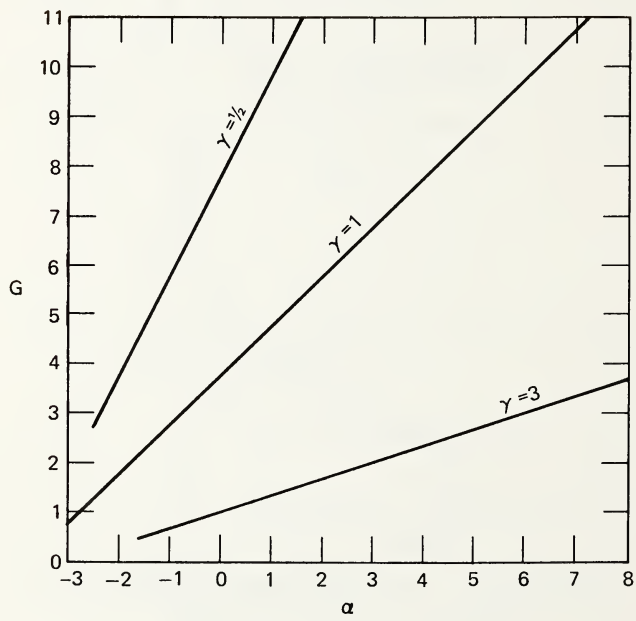


Figure 4-3. Relationship between the coefficients of the modified gamma distribution and the exponential factor G .

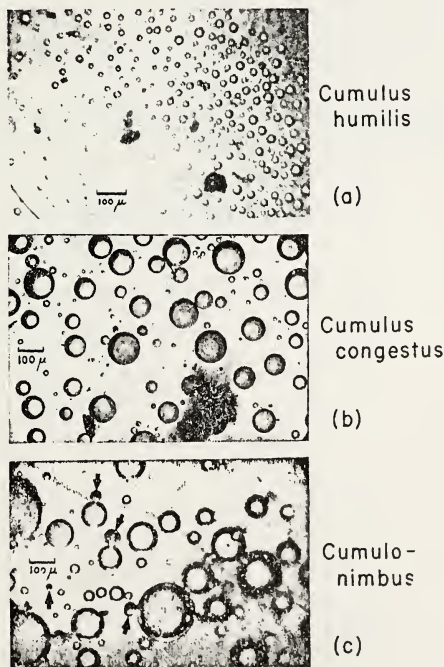


Figure 4-4. Samples of natural drop-size distributions in various clouds.
(Weickmann and aufm Kampe, 1953).

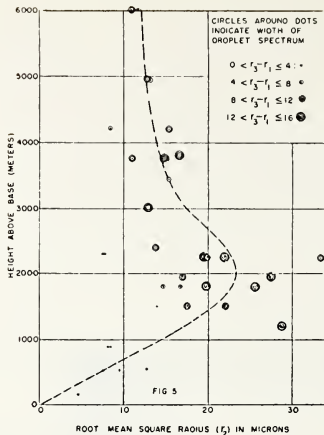


Figure 4-5. Root-mean-square radii in cumuliform clouds versus height above base. (Weickmann and aufm Kampe, 1953).

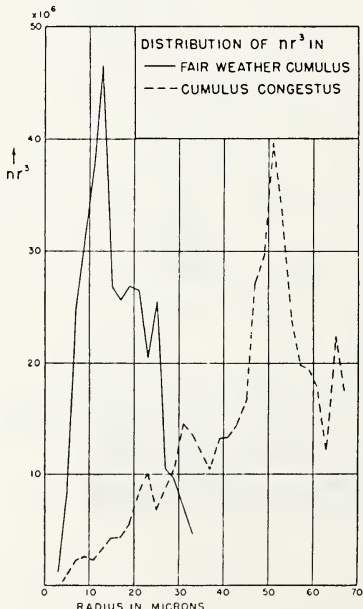


Figure 4-6. Water-content spectra in fair-weather cumulus and cumulus congestus. (Weickmann and aufm Kampe, 1953).

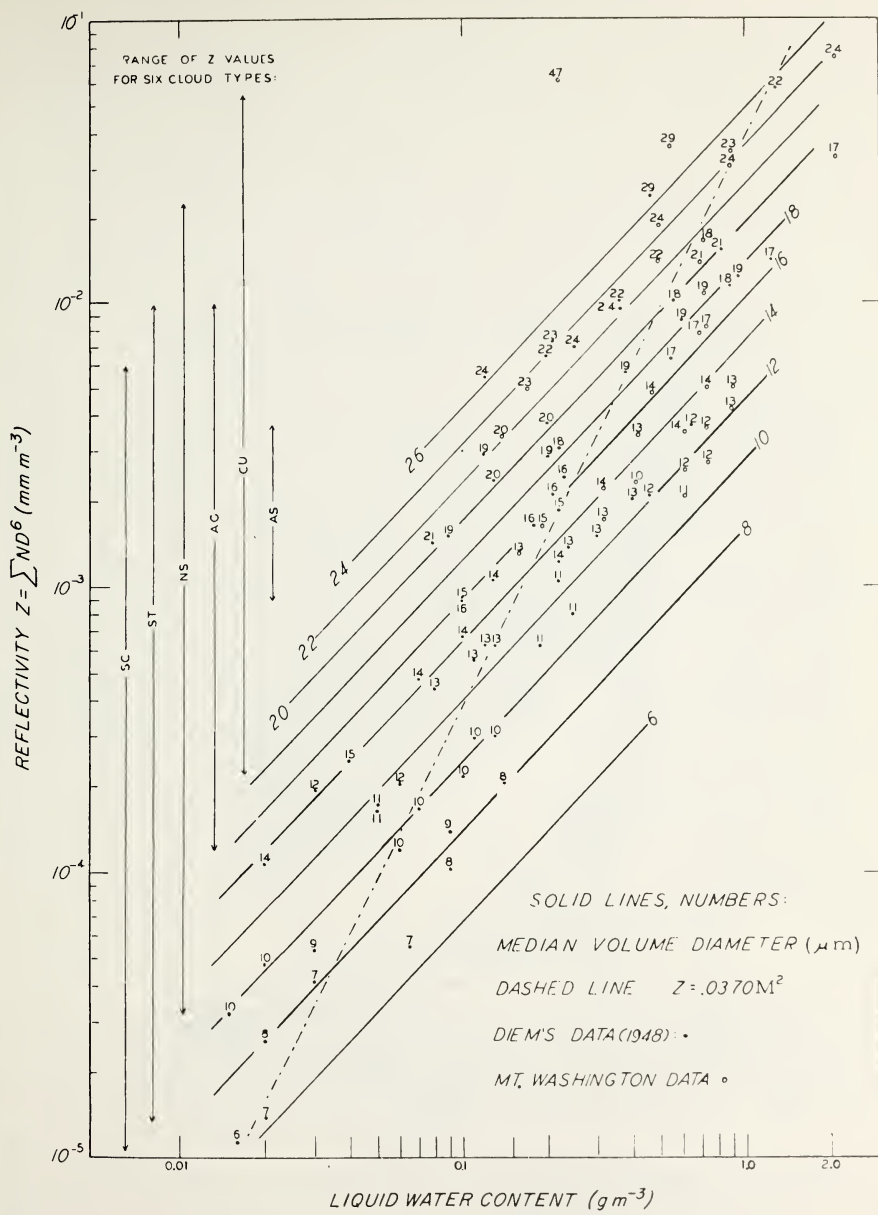


Figure 4-7. Diagram showing the correlation between radar reflectivity factor, the median volume diameter and the liquid water content for clouds, based on 38 impinger observations at Mt. Washington N.H., and 67 aircraft observations by Diem in Germany. (Boucher, 1952)

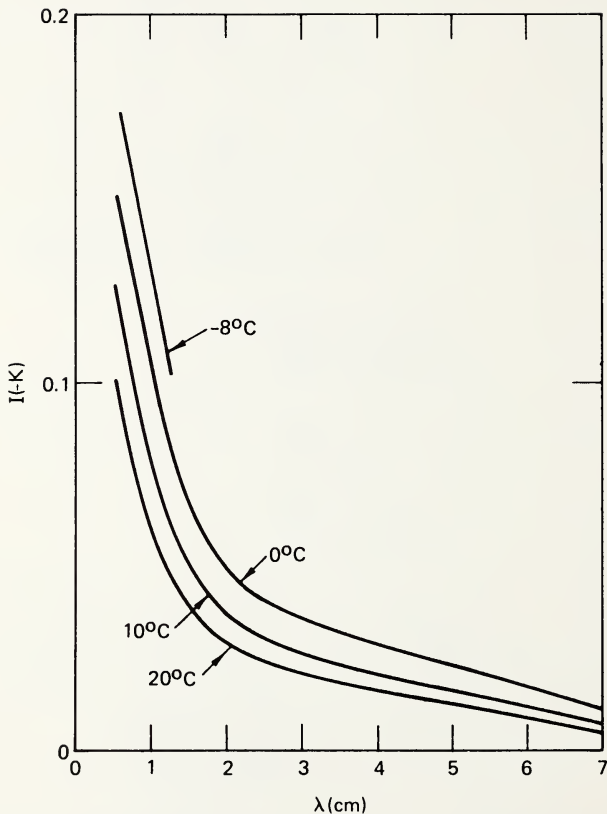


Figure 5-1. Imaginary part of $-K = -(m^2 - 1)/(m^2 + 2)$ as a function of wavelength and temperature.

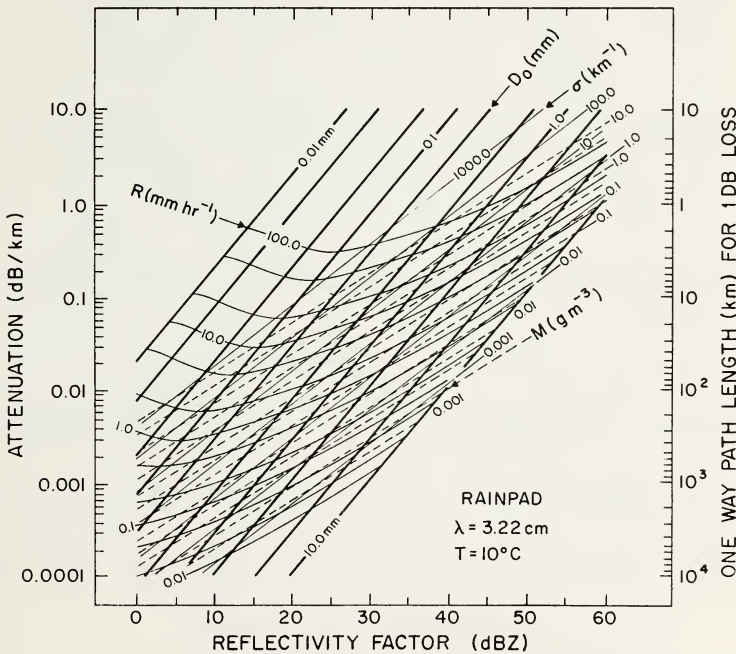


Figure 5-2. RAINPAD diagram of Atlas and Ulbrich (1974) graphically demonstrating relationships between attenuation A, reflectivity factor Z, total mass of liquid water M, rainfall rate R, and optical extinction coefficient σ . Calculations assume a Marshall-Palmer distribution and fit a power law $M = lA^{\beta}$ to the Mie scattering solution. Temperature and wavelength must be assumed.

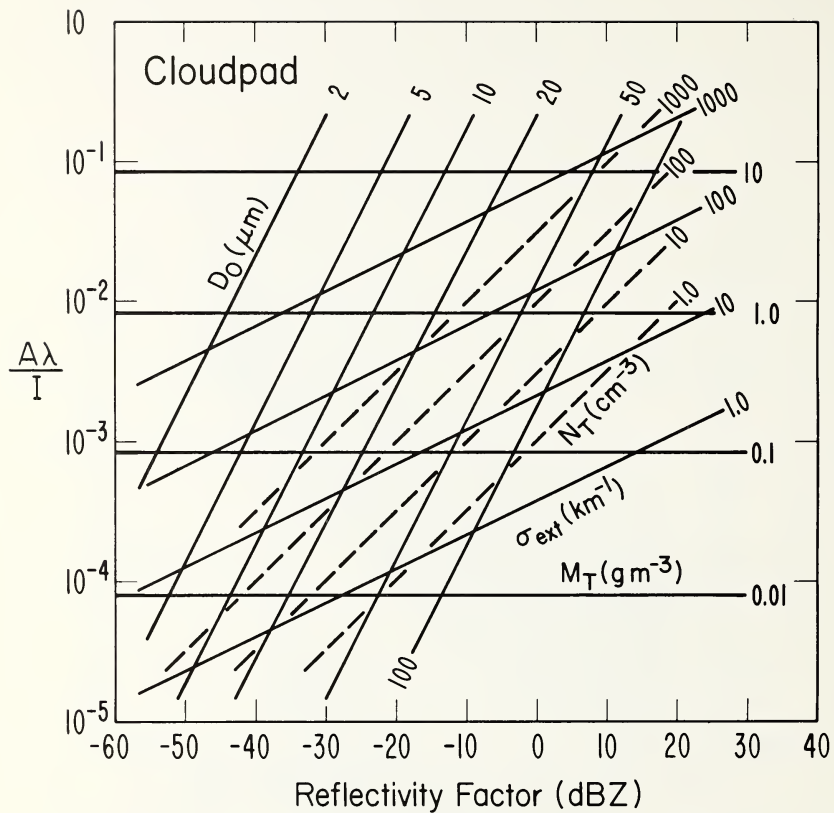


Figure 5-3. CLOUDPAD diagram in which Rayleigh scattering is assumed. Shows relationships between attenuation A, reflectivity factor Z, total mass of liquid water M_T , total number density N_T and optical extinction coefficient σ_{ext} . When attenuation is plotted as the dimensionless quantity $A\lambda/I$, diagram applies for all temperatures and wavelengths. The quantity $I = \text{Imaginary part of } -(m^2/m^2 + 2)$.

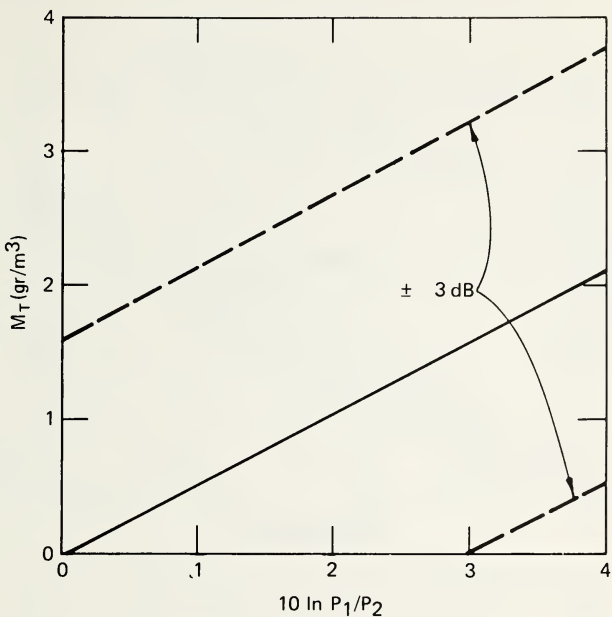


Figure 5-4a. Error in calculation of mass of liquid water assuming an error of $\pm 3 \text{ dB}$ in measured power difference between radars of two different wavelengths.

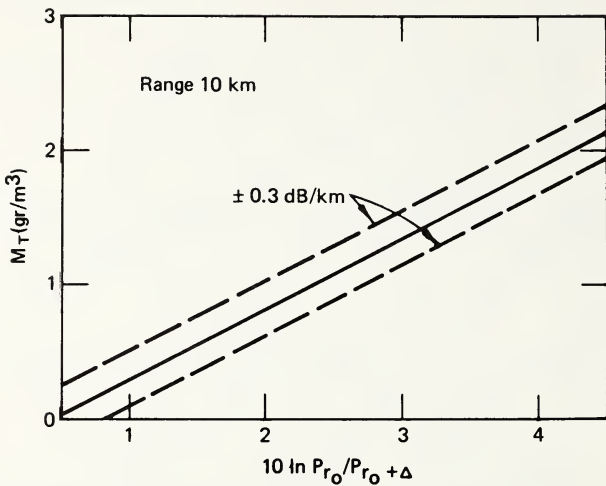


Figure 5-4b. Error in calculation of mass of liquid water assuming an error $\pm 0.3 \text{ dB/km}$ in measured attenuation between ranges r_o and $r_o + \Delta$.

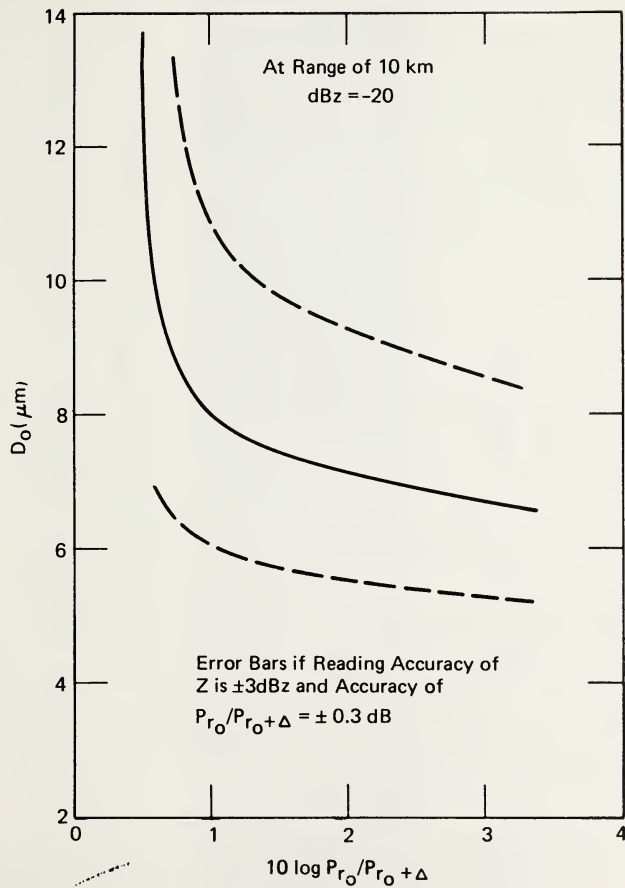


Figure 5-5a. Error in calculation of median mass diameter for assumed conditions indicated on figure.

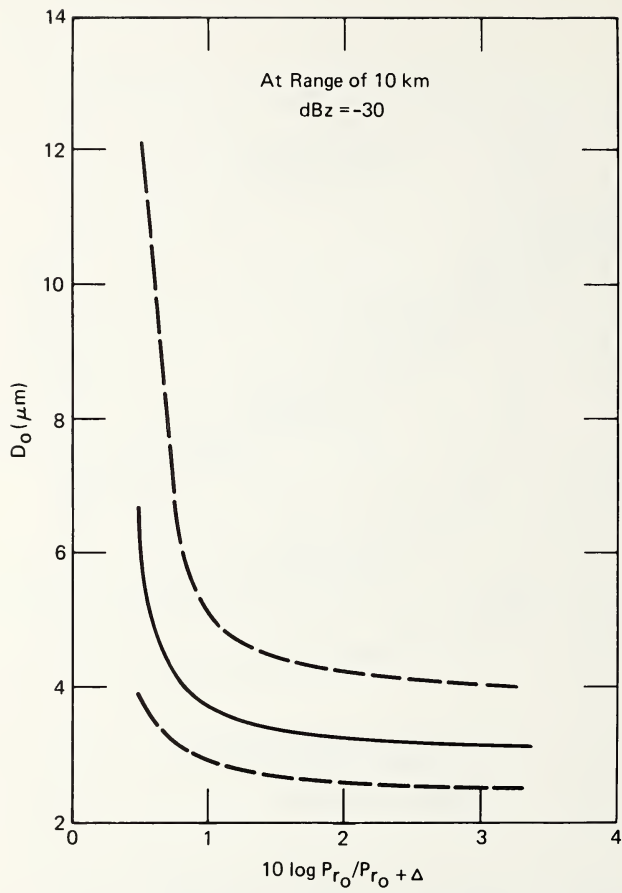


Figure 5-5b. Error in calculation of median mass diameter for an assumed reflectivity of dBZ = -30. Conditions otherwise as in Figure 5-5a.

FRASER, COLO. 11 FEB 1975
Height interval 0-2250 m



Figure 6-1. Sample of vertically pointing radar record showing backscattered returns from cloud ice crystals and also showing faint return from clear-air backscatter seen as faint braided structure at height of 2 km.

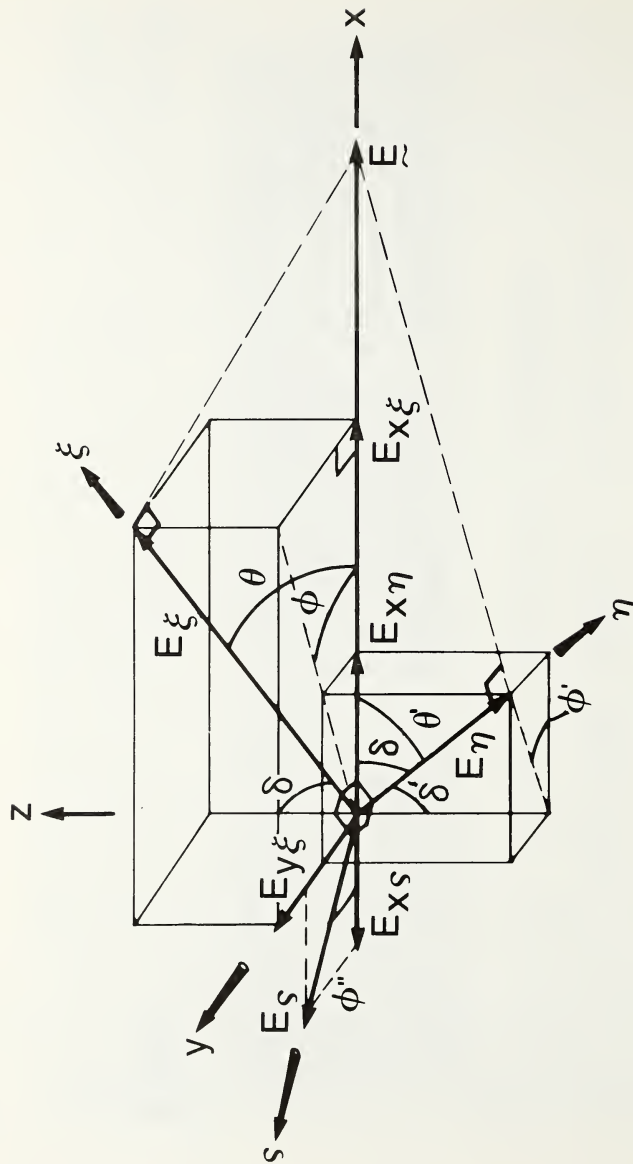


Figure 6-2. Schematic illustration of assumed geometry defining symbols and quantities used in polarization analysis.

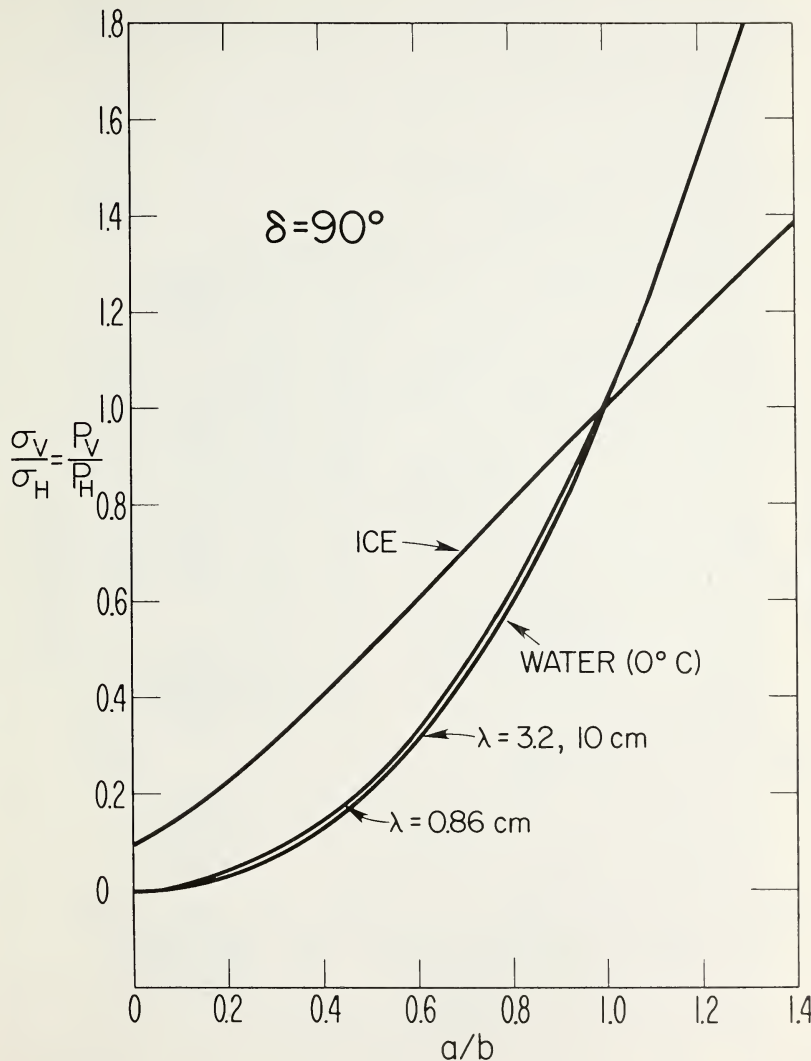


Figure 6-3. Relationship between drop-shape (a/b) and ratio of backscattered power at vertical and horizontal polarizations for horizontal propagation.

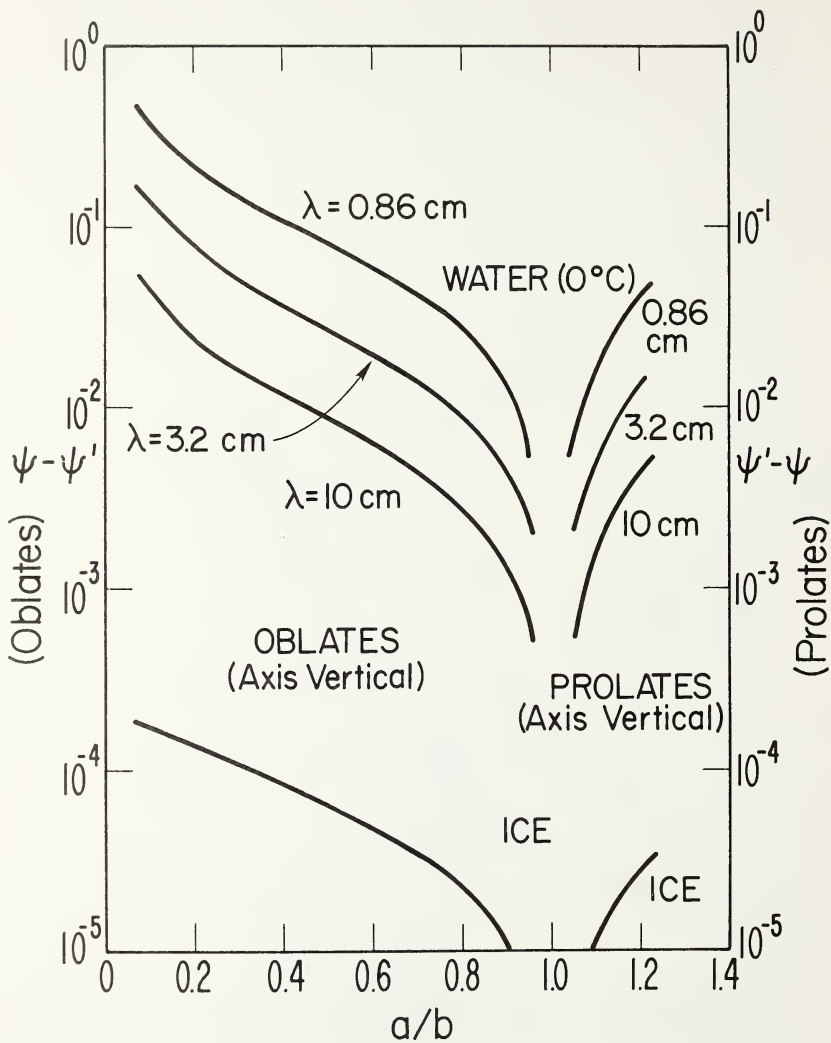


Figure 6-4. Relationship between drop-shape (a/b) and phase difference between vertical and horizontal polarizations for horizontal propagation ($\delta = 90^\circ$).



Typical shape of small water drops falling at terminal velocity (from left to right a_0 : 432, 393, 354, 282, 155.5, 130 \times 0, 44 \times 5, 35 \times 8 μm corresponding to the following values for V_x : 351, 319, 289, 229, 119, 98, 21, 14 cm s^{-1} .



Typical shape of large drops falling at terminal velocity (from left to right a_0 : 4000, 3467.5, 2990, 2665, 1725, 133 mm corresponding to the following values for V_x : 920, 920, 917, 913, 846, 770 cm s^{-1} .

Figure 6-5, 6-6. Photographs of shape of small water drops falling at terminal velocity in the laboratory for various mean radii, a_0 . (From Pruppacher and Beard, 1969).

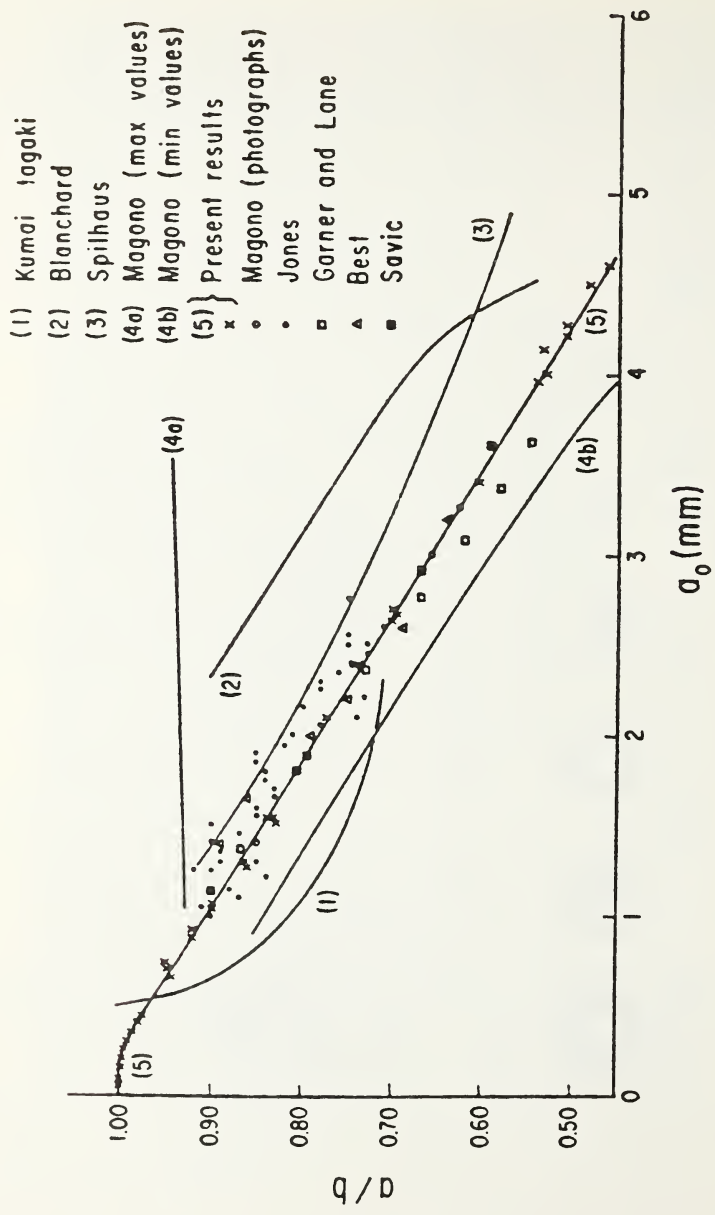


Figure 6-7. Drop deformation versus drop-size from sources indicated on figure.

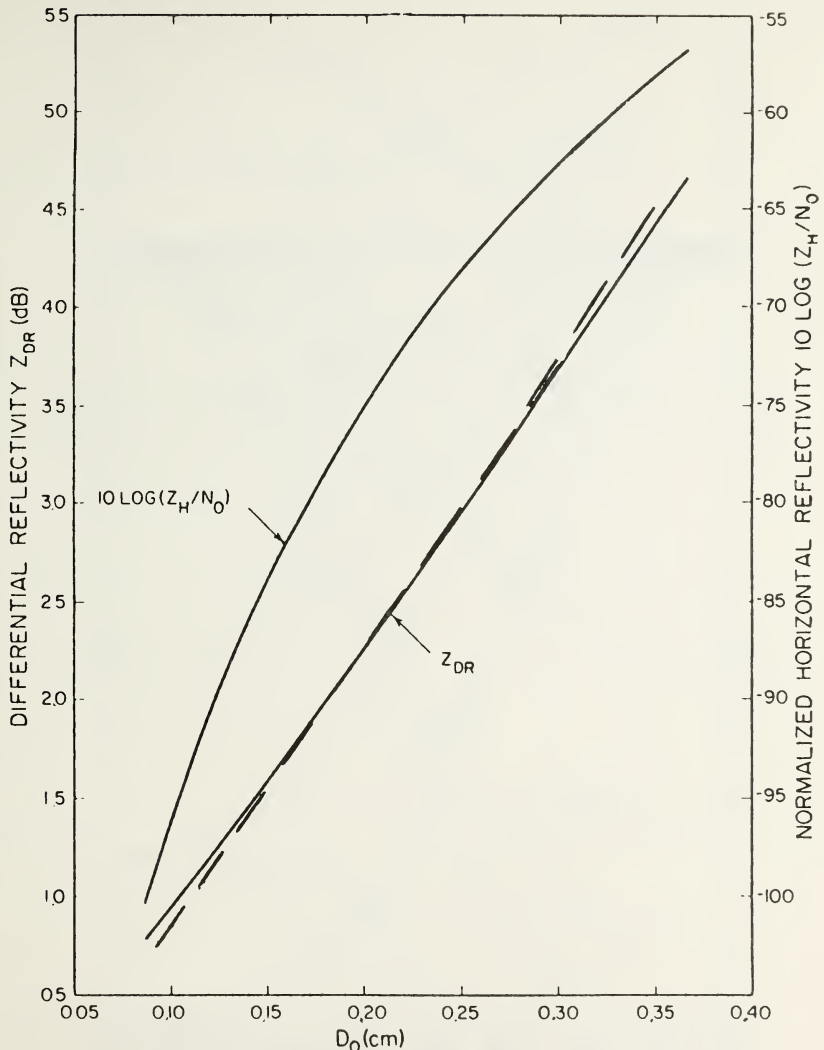


Figure 6-8. Variations of Z_{DR} and normalized horizontal reflectivity $10 \log (Z_H/N_0)$ with D_0 . The drop-size distribution is assumed to be exponential with coefficient N_o . Dashed curve is obtained from Eqs. (6-18a and 6-19b) by assuming a homogeneous distribution of drops by rescaling D_0 .

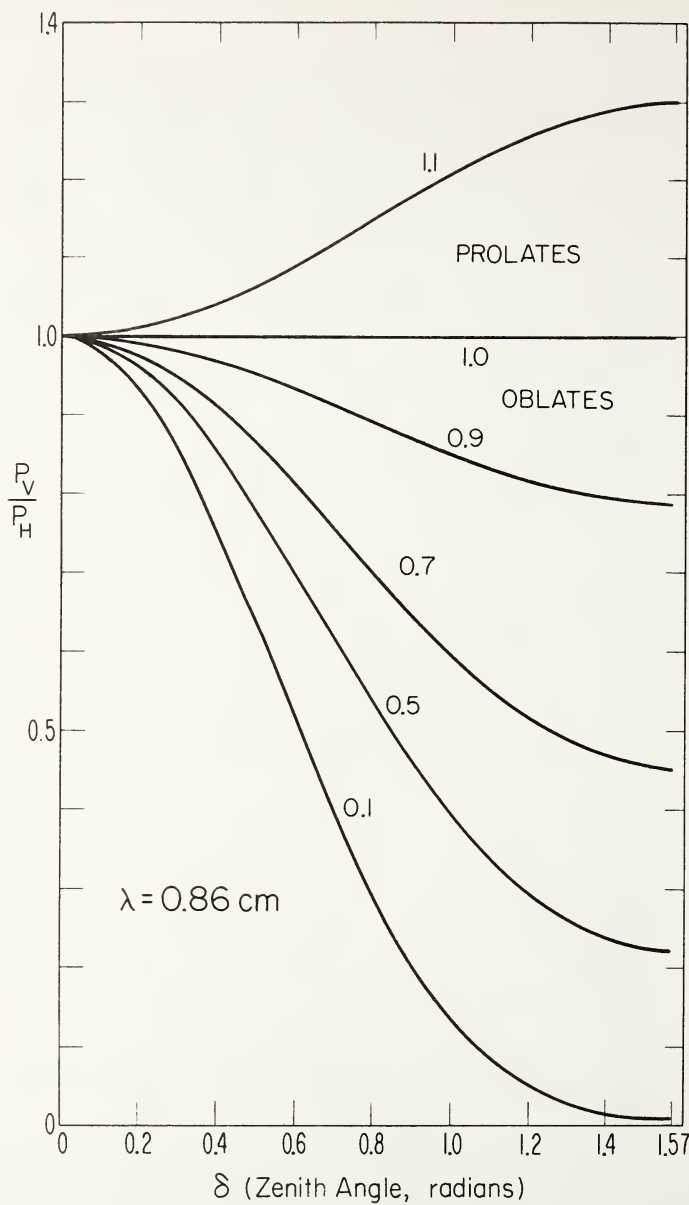


Figure 6-9. Ratio of backscattered power in vertical and horizontal polarizations for various zenith angles assuming spheroidal scatterers whose axes of symmetry are vertical. Plot is parametric in the ratio a/b . Conditions otherwise as indicated on figure.

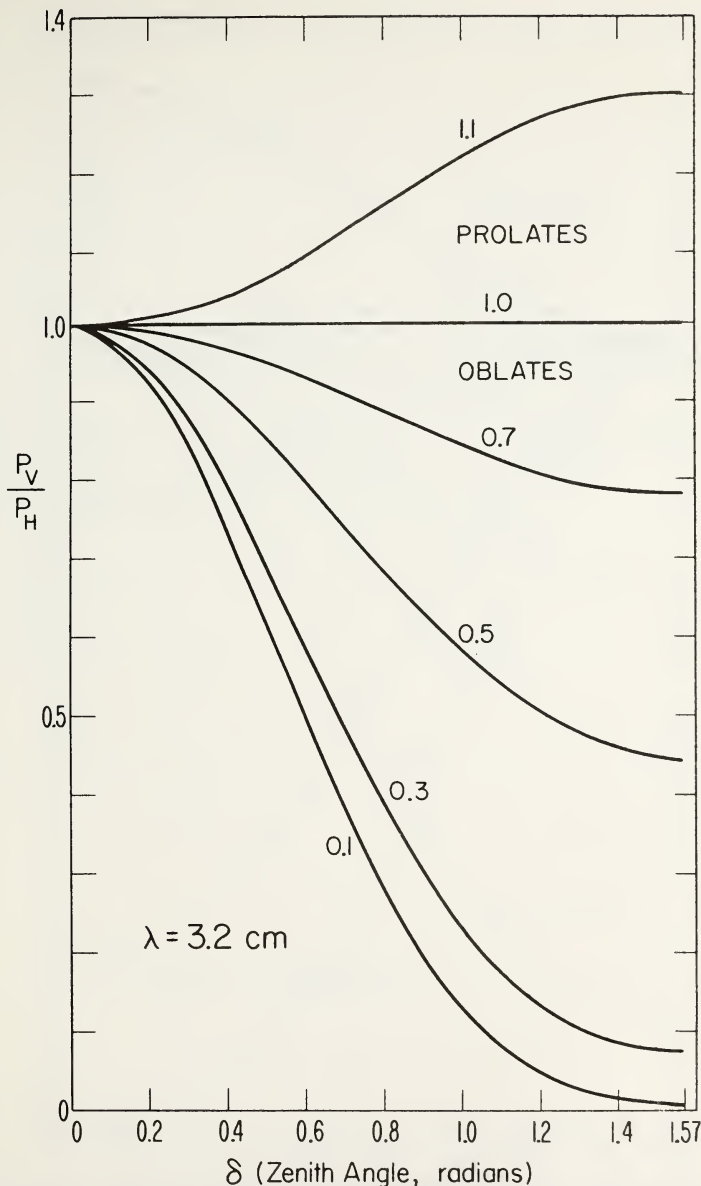


Figure 6-10. Ratio of backscattered power in vertical and horizontal polarizations for various zenith angles assuming spheroidal scatterers whose axes of symmetry are vertical. Plot is parametric in the ratio a/b . Conditions otherwise as indicated on figure.

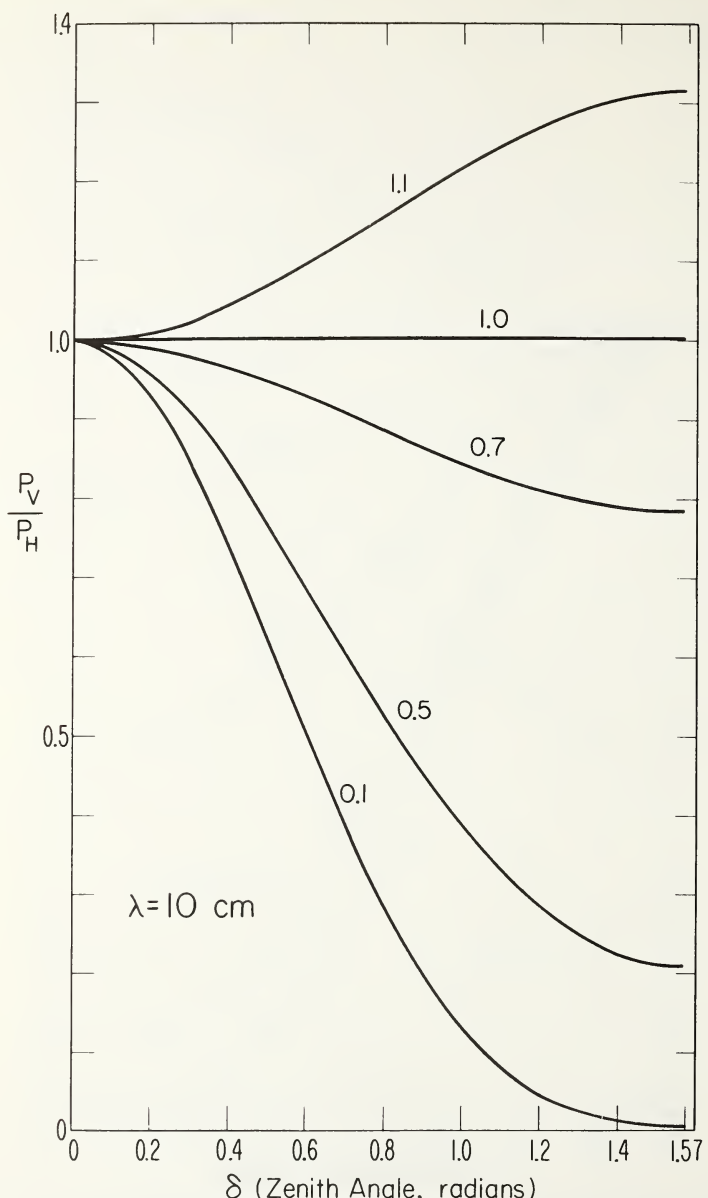


Figure 6-11. Ratio of backscattered power in vertical and horizontal polarizations for various zenith angles assuming spheroidal scatterers whose axes of symmetry are vertical. Plot is parametric in the ratio a/b . Conditions otherwise as indicated on figure.

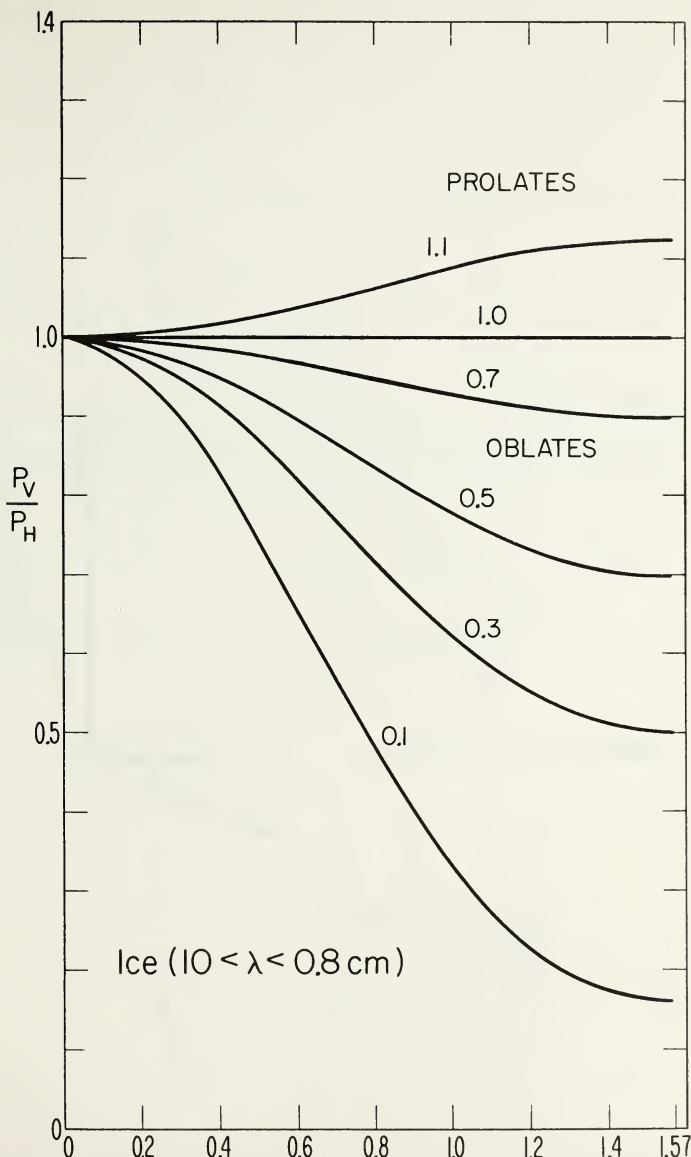


Figure 6-12. Ratio of backscattered power in vertical and horizontal polarizations for various zenith angles assuming spheroidal scatterers whose axes of symmetry are vertical. Plot is parametric in the ratio a/b . Conditions otherwise as indicated on figure.

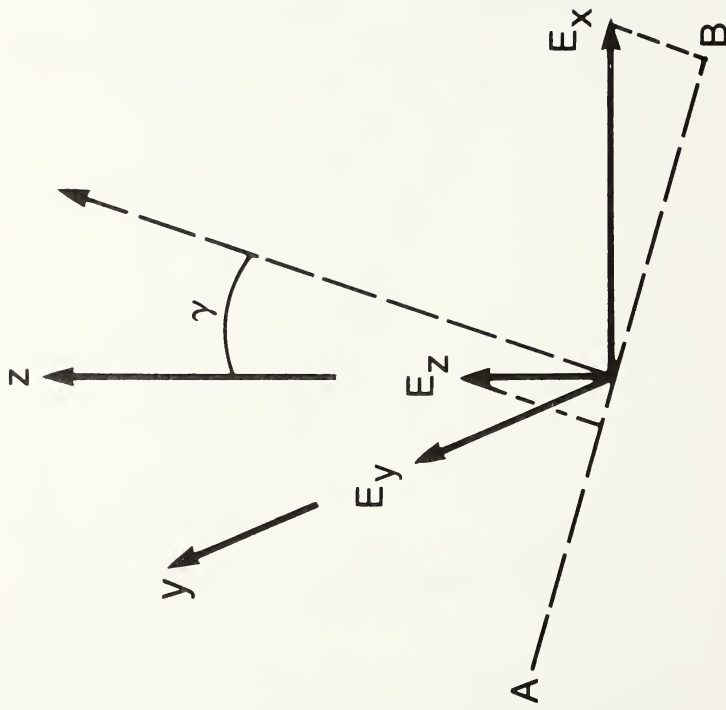


Figure 6-13. Geometry of off-path scattering in arbitrary direction γ .

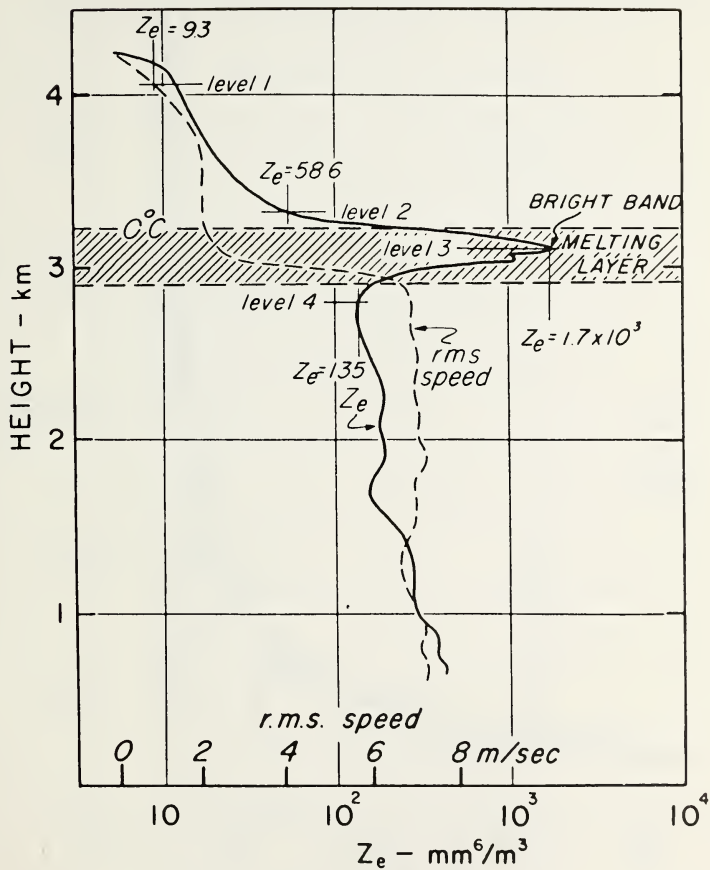


Figure 6-14. Simultaneous profiles of reflectivity factor Z and root-mean-square particle-fall speed in light (1 mm/hr), steady precipitation with bright band. (From Lhermitte and Atlas, 1963).

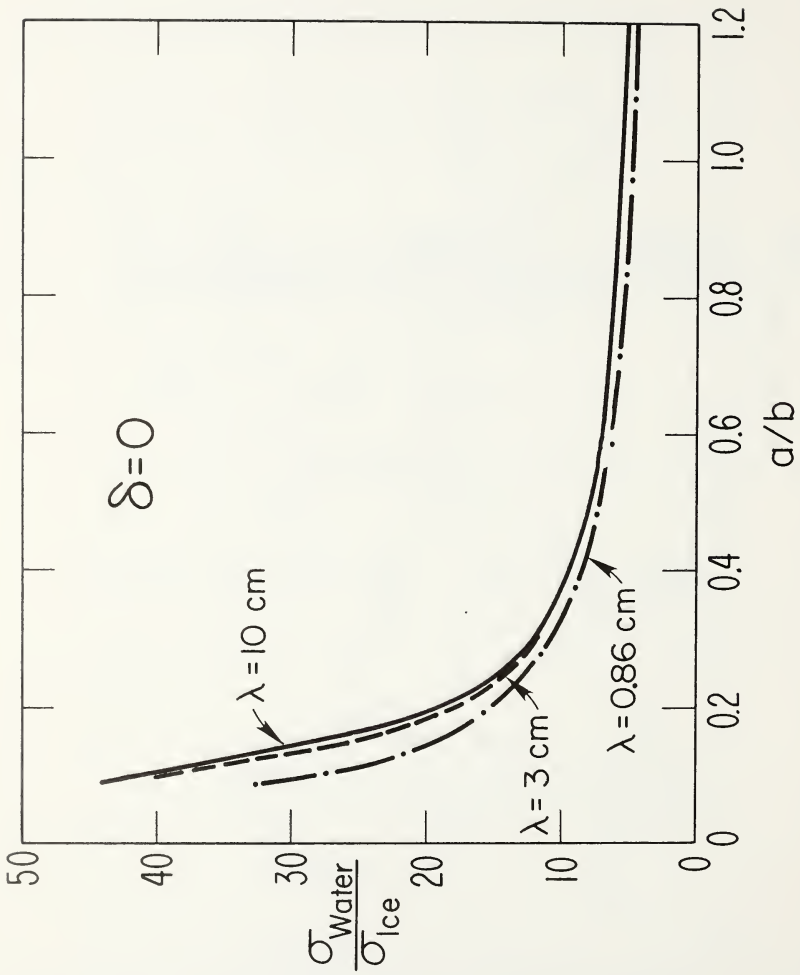


Figure 6-15. Ratio of backscattering cross-section for water and ice particles as a function of shape assuming vertically pointing radar.

TABLE I. RADAR PARAMETERS

*	FMCW	Pulse Doppler NSSL	Pulse Doppler Definor	Pulse Doppler Wallops S.	WSR 57 1-Hook Model	APS 24	TPO 11	TPO 6	CPS 9	OSN 5	K Band (IR55.3)	Chirpka Radar
$P_1(w)$	200(mV)	0.25×10^5	4.7×10^5	7×10^5	2×10^6	4.1×10^5	0.11×10^5	1.2×10^5	0.125×10^5	0.75×10^5	0.25×10^5	3.2×10^6
$P_1(\text{dBm})$	155	103	111.2	110	110	-100	-108	-88	99	-104	89	128
$\lambda(\text{cm})$	10	3.22	10.7	10.7	10.7	10.3	10.3	1.25	0.86	0.86	1.25	23.25
$A_0(\text{m}^2)$	2.54	4.02	31	270	146	5.8	5.8	2.54	1.8	1.8	1.2	310
$\Delta t(\text{ms})$	100	75	150	188	195	75	600	75	150	75	30	22.5
$R(\text{km})$	10	10	10	10	10	10	10	10	10	10	10	1500
$\gamma_{\text{lim}}(1)$	1.8×10^{-14}	1.9×10^{-11}	9.8×10^{-15}	7.9×10^{-16}	5.9×10^{-16}	1.6×10^{-12}	3.1×10^{-14}	1.3×10^{-9}	2.2×10^{-11}	1.7×10^{-9}	8.3×10^{-12}	3.0×10^{-19}
$\gamma_{\text{lim}}(2)$	9.9×10^{-16}	7.3×10^{-13}	5.6×10^{-16}	4.6×10^{-17}	2.9×10^{-17}	9.0×10^{-14}	1.8×10^{-15}	3.8×10^{-11}	5.5×10^{-13}	1.3×10^{-9}	1.2×10^{-8}	3.3×10^{-10}
$\gamma_{\text{lim}}(2.5)$	2.1×10^{-14}	1.6×10^{-11}	1.2×10^{-14}	9.9×10^{-16}	6.2×10^{-16}	1.9×10^{-12}	3.8×10^{-14}	8.1×10^{-10}	1.2×10^{-11}	4.2×10^{-11}	2.1×10^{-13}	2.2×10^{-19}
$\gamma_{\text{lim}}(2.2)$	2.1×10^{-14}	1.6×10^{-11}	1.2×10^{-14}	9.9×10^{-16}	6.2×10^{-16}	1.9×10^{-12}	3.8×10^{-14}	8.1×10^{-10}	1.2×10^{-11}	4.2×10^{-11}	2.1×10^{-13}	2.2×10^{-19}
$\gamma_{\text{lim}}(2.3)$	2.1×10^{-14}	1.6×10^{-11}	1.2×10^{-14}	9.9×10^{-16}	6.2×10^{-16}	1.9×10^{-12}	3.8×10^{-14}	8.1×10^{-10}	1.2×10^{-11}	4.2×10^{-11}	2.1×10^{-13}	2.2×10^{-19}
$\gamma_{\text{lim}}(2.1)$	2.1×10^{-14}	1.6×10^{-11}	1.2×10^{-14}	9.9×10^{-16}	6.2×10^{-16}	1.9×10^{-12}	3.8×10^{-14}	8.1×10^{-10}	1.2×10^{-11}	4.2×10^{-11}	2.1×10^{-13}	2.2×10^{-19}
$\gamma_{\text{lim}}(2.0)$	2.1×10^{-14}	1.6×10^{-11}	1.2×10^{-14}	9.9×10^{-16}	6.2×10^{-16}	1.9×10^{-12}	3.8×10^{-14}	8.1×10^{-10}	1.2×10^{-11}	4.2×10^{-11}	2.1×10^{-13}	2.2×10^{-19}
$\gamma_{\text{lim}}(1.5)$	6.2×10^{-3}	7.15×10^{-3}	4.5×10^{-3}	3.65×10^{-4}	2.3×10^{-4}	0.625	1.2×10^{-2}	0.114	4.2×10^{-4}	3.2×10^{-2}	1.6×10^{-4}	0.025
$\tau(\mu\text{sec})$	0.5	1	1.25	1.3	0.5	4	0.8	0.5	1	0.5	0.2	0.15
$\Upsilon(\mu\text{sec})$	512	768	1250	960	1520	6097	1250	1060	2033	1074	500	3400
Antenna (m)	2.44	3.05	8.5	25	18.4	3.65	2.44	2.14	2.14	2.14	1.22	1.0
Beamwidth (deg)	0.86	1.1	0.33	0.50	2.0	0.37	0.25	0.25	0.25	0.52	1.1	0.6

Table 11. PARAMETERS OF MODIFIED GAMMA DISTRIBUTION
FOR SOME HYDROMETERS AND AEROSOLS
(Deirmendjian's values except as otherwise indicated)

α	γ	$r_c(m)$	$D_0(m)$	$N_f(m^{-3})$	G	a	b	$Vp(m^{3}m^{-3})$	$Z(mm^{6}m^{-3})$	$\sigma_{ext}(m^{-1})$
Haze (Continental)	2	1/2	.07x10 ⁻⁶	1.19x10 ⁻⁶	100x10 ¹⁶	11.669	4.975x10 ³²	15.119x10 ³	1.17x10 ⁻¹¹	NA
Haze (Maritime)	1	1/2	.05x10 ⁻⁶	2.34x10 ⁻⁶	100x10 ¹⁶	9.670	5.333x10 ²²	8.944x10 ³	4.95x10 ⁻¹¹	NA
Haze (High Altitude)	2	1	.10x10 ⁻⁶	0.57x10 ⁻⁶	100x10 ¹⁶	5.671	4.000x10 ²⁹	20.000x10 ⁶	3.14x10 ⁻¹²	NA
Cloud (MOP **)	8	3	2x10 ⁻⁶	4.45x10 ⁻⁶	100x10 ¹⁶	3.677	5.5556x10 ⁶⁰	3.333x10 ¹⁷	3.77x10 ⁻⁹	6.91x10 ⁻⁷
Cloud (Double Corona)	8	3	2x10 ⁻⁶	4.45x10 ⁻⁶	100x10 ¹⁶	3.677	5.5556x10 ⁶⁰	3.333x10 ¹⁷	3.77x10 ⁻⁸	6.91x10 ⁻⁷
Cloud (Corona)	8	3	4x10 ⁻⁶	8.90x10 ⁻⁶	100x10 ¹⁶	3.677	1.0851x10 ⁵⁸	4.17x10 ¹⁶	3.02x10 ⁻⁸	4.42x10 ⁻⁵
Cloud (Cumulus)	6	1	NA	12.89x10 ⁻⁶	100x10 ¹⁶	9.670	2.3730x10 ⁴⁸	1.50x10 ⁶	6.255x10 ⁻⁸	3.74x10 ⁻⁴
Rain * (Drizzle)	0	1	NA	667x10 ⁻⁶	1450	3.673	8x10 ⁶	5.5x10 ³	2.74x10 ⁻⁸	3.77x10 ⁻⁷
Rain * (Light, 1 mm hr ⁻¹)	0	1	NA	900x10 ⁻⁶	1960	3.673	8x10 ⁶	4.1x10 ³	9.09x10 ⁻⁸	3.07x10 ²
Rain * (Moderate, 4 mm hr ⁻¹)	0	1	NA	1200x10 ⁻⁶	2610	3.673	8x10 ⁶	3.1x10 ³	2.87x10 ⁻⁷	2.30x10 ³
Rain * (Heavy, 16 mm hr ⁻¹)	0	1	NA	1600x10 ⁻⁶	3490	3.673	8x10 ⁶	2.3x10 ³	9.08x10 ⁻⁷	1.72x10 ⁴
Snow * (Moderate)	0	1	NA	2980x10 ⁻⁶	930	3.673	1.14x10 ⁶	1.2x10 ³	1.56x10 ⁻⁶	1.91x10 ⁵
Rain (Maritime)	1	1/2	50x10 ⁻⁶	2338x10 ⁻⁶	1000	9.670	0.533x10 ¹²	2.828x10 ²	4.95x10 ⁻⁷	1.83x10 ⁴
Rain (Continental)	2	1/2	70x10 ⁻⁶	1191x10 ⁻⁶	1000	11.669	4.98x10 ¹⁶	4.781x10 ²	1.17x10 ⁻⁷	1.33x10 ³

* From stratiform rainfall rate relations given by Gunn and Marshall (1958) assuming Marshall-Palmer distribution.

** Mother of Pearl
*** Volume of particulates per cubic meter, snow is volume of equivalent spherical liquid drop.

Table III. Cloud Parameters

Cloud type	Number density (N) (m^{-3})	Water content (M) (gr m^{-3})	Reflectivity Z ($\text{mm}^6 \text{ m}^{-3}$)	Median diameter (D_o) (m)	6th power mean diameter (m)	Atlas Barthoff (2) Z ($\text{mm}^6 \text{ m}^{-3}$)	$N_T D_o^6$ (m^{-3})
Fair weather cumulus	302×10^6	1.0		32×10^{-6}		0.0845	
Cumulus congestus	64×10^5	3.9		10.8×10^{-6}		12.7	
Cumulonimbus	72×10^6	2.5		10.8×10^{-6}		8.1	
$\sum_i N_i$ (m^{-3})	$\sigma \sum_i N_i D_i^3$ (gr m^{-3})	$\sum_i N_i D_i^6$ ($\text{mm}^6 \text{ m}^{-3}$)					
Continental cumulus	4.95×10^6	0.35	1.82×10^{-3}	13.2×10^{-6}	12.4×10^{-6}	2.1×10^{-3}	2.6×10^{-3}
Trade cumulus	72.5×10^6	0.81	5.3×10^{-2}	26.5×10^{-6}	30.0×10^{-6}	3.9×10^{-2}	2.5×10^{-2}
Convective cumulonimbus	23.3×10^6	0.335	4.0×10^{-2}	34.0×10^{-6}	34.7×10^{-6}	3.4×10^{-2}	3.6×10^{-2}
Stratiform	5.2×10^6	0.523	1.35	92.0×10^{-6}	80.0×10^{-6}	1.05	3.15

Table IV

<u>Diem's cloud types</u>	$\frac{\pi}{6} \sum_i N_i D_i^3$ <u>(gr m⁻³)</u>	$\sum_i N_i D_i^6$ <u>Z (mm⁶ m⁻³)</u>	D_o <u>(m)</u>
CU ₁	0.32	1.18×10^{-3}	11.2×10^{-6}
CU ₂	0.87	2.76×10^{-2}	20.6×10^{-6}
SC	0.09	3.53×10^{-4}	10.1×10^{-6}
AS	0.28	2.40×10^{-3}	12.8×10^{-6}
NS	0.40	1.40×10^{-2}	23.4×10^{-6}
ST	0.29	1.29×10^{-2}	24.1×10^{-6}

Table V.
South Park Cumulus

N_T (cm^{-3})	\bar{D} (μm)	M (gr m^{-3})	D_o (μm)	Z ($\text{mm}^6 \text{m}^{-3}$)
687	8.4	.216	30.8	.0163
72	7.4	.015	27.2	7.8×10^{-4}
487	9.7	.234	35.6	2.7×10^{-2}
565	9.3	.236	34.1	2.4×10^{-2}
461	9.9	.233	36.3	2.9×10^{-2}
559	9.7	.405	35.5	4.7×10^{-2}
104	7.1	.028	26.1	1.3×10^{-3}
64	8.3	.027	30.5	2.0×10^{-3}
209	8.1	.085	29.7	5.8×10^{-3}
352	9.5	.234	34.9	2.6×10^{-2}

Table VI. Observed Plume Data

Droplet Diameter (m)	Sample Identifier						#7
	#1	#2	#3	#4	#5	#6	
1	69	164	666	183			
2							
3							
4							
5	363	366	732	289	27	56	36
6							
7							
8	374	486	659	361	90	86	72
9							
10	466	427	792	897	123	115	96
11							
12							
13	95	295	390	370	104	120	107
14							
15	8	143	216	99	23	66	25
16							
17							
18	21	33	47	2	17	2	
19							
20		18			12	2	
Plume Temp (°C)	20	20	20	20	20	20	20
Air Temp (°C)	5.8	5.8	5.8	5.8	16.6	16.6	16.6
Pressure (mb)	990	990	990	990	990	990	990
Water Vapor Density (gr m ⁻³)	4.06	4.06	4.06	4.06	8.3	8.3	8.3
N _T (m ⁻³)	3664x10 ⁶	5151x10 ⁶	9566x10 ⁶	5808x10 ⁶	963.5x10 ⁶	1210x10 ⁶	897.5x10 ⁶
V _T (m ³ m ⁻³)	2.54x10 ⁻⁶	5.57x10 ⁻⁶	8.91x10 ⁻⁶	7.37x10 ⁻⁶	1.36x10 ⁻⁶	2.165x10 ⁻⁶	1.32x10 ⁻⁶
Z _T (mm m ⁻³)	3.45x10 ⁻³	1.45x10 ⁻²	2.66x10 ⁻²	2.13x10 ⁻²	3.01x10 ⁻³	7.93x10 ⁻³	3.15x10 ⁻³

REFERENCES

- Agee, E. M., (1971). An artificially induced snowfall. *Bull. Amer. Meteor. Soc.*, 52, 557-560.
- Atlas, David, (1964). Advances in radar meteorology. *Adv. in Geophysics*, 10, 478 p.
- Atlas, David, (1954). The estimation of cloud parameters by radar. *J. of Meteorl.*, 11, 309-317.
- Atlas, David and Shepard Bartnoff, (1953). Cloud visibility, radar reflectivity, and drop-size distribution. *J. of Meteorl.*, 10, 143-148.
- Atlas, David, Milton Kerker, and Walter Hitschfeld, (1953). Scattering and attenuation by non-spherical atmospheric particles. *J. Atmos. and Terrestrial Physics*, 3, 108-119.
- Atlas, David, and Ulbrich, C. W., (1974). The physical basis for attenuation rainfall relationships and the measurement of rainfall parameters by combining attenuation and radar methods. *J. de Recherches Atmos.*, 3, 275-298.
- Austin, P. M., and Bemis, A. C., (1950). A quantitative study of the "bright band" in radar precipitation echoes. *J. Meteorl.*, 7, 145-51.
- Bartnoff, S., and Atlas, D., (1951). Microwave determination of particle-size distribution. *J. Meteorl.*, 8, 130-131.
- Battan, Louis J., (1973). Radar Observation of the Atmosphere, The Univ. of Chicago Press, 324 p.
- Bean, B. R., and Dutton, E. J., (1966). Radio Meteorology. U. S. Government Printing Office, Washington, DC, 431 p.
- Best, A. C., (1951). Drop size distribution in cloud and fog. *Quart. J. Roy. Meteorl. Soc.*, 77, 418-426.
- Bolgiano, R., (1958). The role of turbulent mixing in scatter propagation. *IRE Trans. on Antennas and Propagation AP-6*, 161-168.
- Booker, H. G., and W. E. Gordon, (1950). A theory of radio scattering in the troposphere. *Proc. of the I.R.E.* pp 401-412.

- Boucher, R. J., (1952). Empirical relationship between radar reflectivity drop size distribution and liquid water content in clouds. Mount Washington Observatory, Contract AF 19(122)-399, 14 p.
- Breed, D. W., L. O. Grant, and J. Dye, (1976). Cloud droplet distribution in high elevation continental cumulis. *Proc. Intern. Conf. on Cloud Physics*, Boulder, CO, 658-664.
- Bringi, V. N., and Seliga, T. A., (1977). Scattering from non-spherical hydrometers. *Proc. Open Symposium, Commission F, URSI*, La Baule, France, 199-204.
- Chernikov, A. A., (1968). Radio wave scattering in clouds and the radar equation. Proceedings of the 3rd All-Union Conference on Radar Meteorology (Moscow) Ed. Kostarev et al. (English translation by Ron Hardin) pp 68-73.
- Cox, D. C., H. W. Arnold, and A. J. Rustako, (1977). Some observations of anomalous depolarization on 19 and 12 GHz earth-space propagation paths. *Radio Sci.*, 12, 435-440.
- Deirmendjian, D., (1969). Electromagnetic Scattering on Spherical Polydispersions. Amer. Elsevier Publishing Co., Inc., New York, 290 p.
- Diem, M., (1948). Messung der Grösse von Wolkenelementen, II. *Meteor. Rundschau*, 1, 261-273.
- Donaldson, R. J., Jr., (1955). Drop-size distribution, liquid water content, optical transmission, and radar reflectivity in fog and drizzle. *Proc. 5th Weather Radar Conf.*, Asbury Park, New Jersey, 275-280.
- Dye, J. E., (1976). Comparisons of the electrostatic disdrometer with impactor slides. *J. Appl. Meteorol.*, 15, 783-789.
- Dye, J. E., (1974). Observations of precipitation development in cumulus congestus clouds on July 9, 1973. *Proc. Conf. on Cloud Physics*, Boston, Mass., 148-151.
- Foote, G. B., and du Toit, P. S., (1969). Terminal velocity of raindrops aloft. *J. Appl. Meteorol.*, 8, 249-253.
- Gans, R., (1912). Über die From ultramiskroskopischer Goldteilchen. *Annalen der Physik*, 37, 881-900.

- Goldhirsh, Julius, and Isadore Katz, (1974). Estimation of raindrop size distribution using multiple wavelength radar systems. *Radio Sci.*, 9, 439-446.
- Gunn, K. L. S., and J. S. Marshall, (1958). The distribution with size of aggregate snowflakes. *J. Meteorol.*, 15, 452-466.
- Gunn, R., and Kinzer, G. D., (1949). The terminal velocity of fall for water droplets in stagnant air. *J. Meteorol.*, 6, 243-48.
- Hanna, S. R., and F. A. Gifford, (1975). Meteorological effects of energy dissipation at large power parks. *Bull. Amer.*, 56, 1069-1076.
- Harper, W. G., (1964). Cloud detection with 8-6 millimetre wavelength radar. *Met. Mag.*, Lond. 93, 337-345.
- Hodkinson, J. R., (1966). The optical measurement of aerosols. *Aerosol Sci.*, C. N. Davies, Ed., Academic Press, New York, 287-357.
- Huff, F. A., (1972). Potential augmentation of precipitation from cooling tower effluents. *Bull. AMS.*, 53, 639-644.
- Imai, I., (1950). On the velocity of falling raindrops. *Geophys. Mag.*, (Tokyo) 31, 244-249.
- Jiusto, J. E., (1974). Remarks on visibility in fog. *J. Appl. Meteor.*, 13, 608-610.
- Kerker, M., Langenberg, M. P., and Gunn, K. L. S., (1951). Scattering of microwaves by a melting spherical ice-particle. *J. Meteorol.*, 8, 424.
- Knollenberg, R. G., (1976). Three new instruments for cloud physics measurements: the 2-D spectrometer, the Axially Scattering spectrometer, and the Active Scattering spectrometer. *Proc. Intern. Cloud Physica Conf.*, Boulder, CO, U.S.A. 554-561.
- Kovasny, L. S. G., M. S. Uberoi, and S. Corrsin, (1949). The transformation between one- and three-dimensional power spectra for an isotropic scalar field. *Phys. Rev.*, 76, 1263-1264.
- Lhermitte, R. M., and Atlas, D., (1963). Doppler fall speed and particle growth in stratiform precipitation. *Proc. Tenth Wea. Radar Conf.*, 297-302.

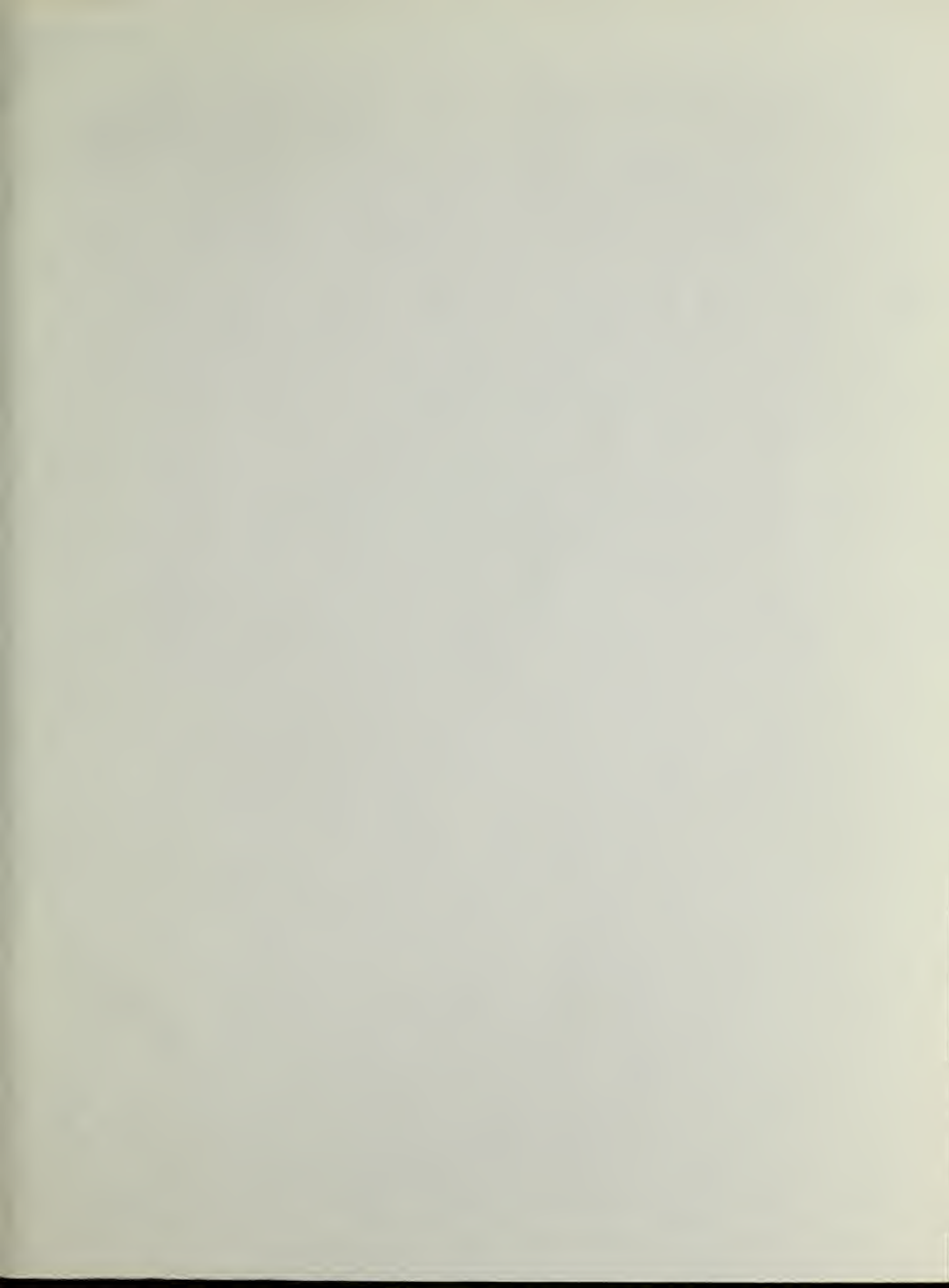
- Marshall, J. S., and W. M. K. Palmer, (1948). The distribution of raindrops with size. *J. Meteor.*, 5, 165-166.
- Mason, B. J., (1957). The Physics of Clouds. Oxford Univ. Press, London and New York, 481 p.
- Naito, K., and D. Atlas (1966). On microwave scatter by partially coherent clouds. Proc. 12th Weather Radar Conference (Boston) pp. 7-12.
- Ottersten, Hans, (1969). Radar backscattering from the turbulent clear atmosphere. *Radio Sci.*, 4, 1251-1255.
- Pena, J. A., (1977). Personal communication, Dept. of Meteorology, the Pennsylvania State University, Univ. Park, PA, 16802.
- Petrocchi, P. J., and W. H. Paulsen, (1966). Meteorological significance of vertical density profiles of clouds and precipitation obtained with the AN/TPQ-11 radar. *Proc. 12th Radar Meteor. Conf.*, Norman, OK 467-472.
- Plank, Vernon G., Atlas, David, and Wilbur H. Paulsen, (1954). The nature and detectability of clouds and precipitation as determined by 1.25 Centimeter radar. *J. Meteor.* 12, 358-378.
- Probert-Jones, J. R., (1962). The radar equation in meteorology. *Quart. J. Roy. Meteorol. Soc.*, 88, 485-495.
- Pruppacher, H. R., and K. V. Beard, (1969). A wind tunnel investigation of the internal circulation and shape of water drops falling at terminal velocity in air. *Quart. J. Roy. Meteor. Soc.*, 96, 247-256.
- Pruppacher, H. R., and R. L. Pitter, (1970). A semi-empirical determination of the shape of cloud and rain drops. *J. Atmos. Sci.*, 28, 86-94.
- Rayleigh, Lord, (1881). Scientific Paper 76, Phil. Mag., 12, 81.
- Ricks, N. R., (1977). A feasibility study for the application of K-band radar in the investigation of cooling tower plumes. NOAA Tech. Memo., ERL-ARL-66, 39 p.
- Seliga, T. A., and V. N. Bringi, (1976). Potential use of radar differential reflectivity measurements at orthogonal polarizations for measuring precipitation. *J. Appl. Meteor.*, 15, 69-76.

- Smith, R. L., (1964). Scattering of microwaves by cloud droplets.
Proc. 11th Weather Radar Conference (Boulder, CO) pp 202-207.
- Squires, P., (1958). The microstructure and colloidal stability of
warm clouds. Pt. I, The relationship between structure and
stability. *Tellus*, 10, 256-261.
- Strauch, R. G., (1976). Theory of Application of the FM-CW Doppler
Radar, Ph.D. Thesis, University of Colorado.
- Tatarski, V. I., (1961). Wave Propagation in a Turbulent Medium,
translated by R. A. Silverman, McGraw-Hill, New York, 285 p.
- Warner, C., (1977). Calculations of backscattering and depolarization by
wet hailstones at 2.88 GHz. Scientific Rept. 17w-90, McGill Univ.,
47 p.
- Waterman, P. C., (1965). Matrix formulation of electromagnetic scattering
Proc. IEEE, 53, 805-812.
- Weickmann, H. K., and H. J. aufm Kampe, (1953). Physical properties of
cumulus clouds. *J. Meteor.* 10, 204-211.
- Wexler, R., (1955). An evaluation of the physical effects in the melting
layer. *Proc. Fifth Wea. Radar Conf.*, Fort Monmouth, NJ, 329-34.









PENN STATE UNIVERSITY LIBRARIES



A000072041093